



MASTER THESIS

Curriculum: Structural Engineering and Offshore Structures	Spring semester, 2021 Open Access
Author: Hamad Alalawi	<div style="border: 1px solid black; background-color: #e0f0ff; padding: 5px; display: inline-block;"> <i>hamad alalawi</i> </div> (author signature)
Faculty supervisor: Gerhard Ersdal External supervisor(s): Michael Muskulus, Sebastian Drexler	
Credits (ECTS): 30 ECTS	
Master thesis title:	Structural reliability and optimal design of fixed jacket of offshore wind turbine
Keywords: <ol style="list-style-type: none"> 1. Structural Reliability 2. Robust Design 3. Gaussian Process 4. Probability Analysis 5. Probabilistic Modelling 	Number of pages: 75 + appendices/other: 1 Stavanger, 15.06.2021 date/year

Acknowledgement

“Always walk through life as if you have something new to learn, and you will.”

-Vernon Howard

I would like to express my gratitude to all of those who helped me to achieve my goal and accomplish this thesis. I want to thank my supervisors: Gerhard Ersdal, Michael Muskulus, and Sebastian Drexler, for all the valuable comments throughout the meetings and all the knowledge they shared with me to make sure I learned the most out of this topic.

I would also like to thank my family, especially my mom, for not stopping to believe in me and support me from the beginning to the very end. Warm thanks to an exceptional person in my life, Elinor, who kept pushing and motivate me to finish my thesis.

Finally, I would like to thank all my friends, especially Tarek, for supporting me, joining the journey with me, and cheering me up.

Abstract

The assessment of structural reliability for offshore wind turbines (OWTs) is challenging. The environmental conditions and loads on a wind turbine have large variability, and wind and wave act simultaneously on the structures, giving rise to combined effects that are difficult to assess. Often a time-domain simulation of the load components is required to assess the loads and the combination of loads. Hence, the minimum of simulations that still produces sufficiently accurate results is beneficial.

The objective of this thesis is to test different methods for estimating the fatigue reliability of a wind turbine structure and particularly seeking methods where a minimum of such load-response simulations is required while maintaining a high level of accuracy. Achieving this objective would require a simplified model of the wind turbine and its substructure, in this case, a jacket structure. This simplified model would allow for implementing an effective way of calculating the loads affecting the system and the response of the wind turbine structure. In this thesis, the fatigue of the substructure of the wind turbine due to wind loading is studied based on pre-performed damage simulations.

Gaussian processes are a relatively new approach to obtaining structural reliability, is presented using a statistical regression model to estimate fatigue damage. Predicting the total wind-induced fatigue damage in the structure is the aim of this research. The method is compared with other methods, such as Monte Carlo Integration and Bins Method, which requires hundreds if not thousands of load-response simulations, which is time-consuming and costly. The results obtained in this thesis show that the adopted Gaussian Process regression approach is applicable to evaluating structural reliability analysis using a small number of training datasets.

Nomenclature

Abbreviation

OWT	Offshore Wind Turbine
SCF	Stress Concentration Factor
PV	Photovoltaics
CV	Coefficient of Variation
NREL	National Renewable Energy Laboratory
FORM	First-Order Reliability Method
FOSM	First-order second-moment
MCI	Monte Carlo Integration
GPR	Gaussian Process Regression
CG	Conjugate gradient
PDF	Probability density function
CDF	Cumulative density function

Roman Symbols

C_D	Drag Coefficient
D	accumulated fatigue damage, Chord diameter
A	Cross-section Area
U	Wind Speed
C_M	Inertia Force Coefficient
V	Volume
t	time
H	wave height
k	wave number

x	direction of propagation
Re	Reynolds number
n_i	number of stress cycles in a stress block i
g	gravitational constant
c	wave phase velocity
u	horizontal particle speed
U	wind velocity
u_{ref}	reference wind velocity
Z	hub height
Z_{ref}	reference height
Z_0	surface roughness
K_r	terrain roughness factor
F_D	drag force
F_L	lifting force
C_L	lift coefficient
C_M	moment coefficient
C_p	surface pressure coefficient
M	mean overturning moment
B	arm reference value
p	static pressure
p_0	velocity pressure
q	dynamic pressure

Greek Symbols

ω	Eigen Frequency
β	d/D
γ	R/T

ρ	density
$\sigma_{nominal}$	Nominal Stress
$\sigma_{hot\ spot}$	Hot Spot Stress
α	L/D , power coefficient
τ	t/T
λ	wavelength
\emptyset	velocity potential
η	water surface elevation
σ	standard deviation
μ	mean
φ	density function

Table of Content

Acknowledgement	2
Abstract	3
Nomenclature	4
Abbreviation	4
Roman Symbols	4
Greek Symbols	5
Chapter 1: Introduction	13
1.1 Wind Turbines	13
1.2 Motivation and Objective	14
1.3 Approach	15
1.4 Structure of the thesis	17
Chapter 2: Background	18
2.1 Offshore wind turbine	18
2.2 Fixed substructures	18
2.3 Power law wind profile	21
2.4 Logarithmic wind profile	22
2.5 Mean and total wind load	26
2.6 Mal functions of components	28
2.7 Fatigue Analysis	29
Chapter 3: Literature Review	35
3.1 Modelling of uncertainties in structural engineering	35
3.2 First-Order Reliability Method (FORM)	38
3.3 First-Order Second-Moment (FOSM) method	39

3.4 Structural Reliability Analysis	40
3.5 Bins Method.....	42
3.6 Monte Carlo Integration.....	43
3.7 Numerical Integration	45
3.8 Gaussian Process.....	45
Chapter 4: Methodology	47
4.1 Wind Distribution	47
4.2 Damage Curve	48
4.3 Total damage estimation	48
4.3.1 Numerical Integration	49
4.3.2 Bins Method.....	49
4.3.3 Monte Carlo Integration.....	49
4.3.4 Failure probability using deterministic value	49
4.3.5 Gaussian Process.....	50
Chapter 5: Results	52
5.1 Damage Estimation.....	52
5.1.1 Damage Estimation Using Bins Method.....	52
5.1.2 Damage Estimation Using Monte Carlo Integration	52
5.1.3 Damage Estimation Using Numerical Integration.....	53
5.1.4 Method Used in the Industry.....	53
5.2 Damage Comparison.....	53
5.3 Reliability estimation	54
5.4 Probability of Failure and Reliability	55
5.5 Gaussian Process.....	55
5.5.1 The strategy of choosing observations.....	57

Chapter 6: Discussion	67
6.1 Effect of Length Scale	67
6.2 Effect of Noise	67
6.3 Convergence	68
Chapter 7: Conclusion, Recommendation, and Further Work.....	70
7.1 Recommendations.....	70
7.1.1 Points Selection.....	70
7.1.2 Convergence	70
7.2 Further Work.....	71
References.....	72
Appendix.....	76
Julia Script	76

List of Figures

Figure 1-1 OC4 Jacket substructure CAD model(a), and simplified tower model(b) (Lai et al., 2016)	15
Figure 2-1 wind profile (Halici and Mutungi, 2016)	21
Figure 2-2 vertical wind shear profile (Maran, Sard 2019)	22
Figure 2-3 wind speed profiles vs static stability in the surface layer (Abdalla et al., 2017)	24
Figure 2-4 seasonal cycle of wind shear (Abdalla et al., 2017)	24
Figure 2-5 Wind speed profiles for different conditions in Summer (Abdalla et al. (2017))	25
Figure 2-6 Wind speed profiles for different conditions in Autumn (Abdalla et al. (2017))	25
Figure 2-7 Wind speed profiles for different conditions in Spring (Abdalla et al. (2017))	25
Figure 2-8 Wind speed profiles for different conditions in Winter (Abdalla et al. (2017))	25
Figure 2-9 main components' share of the total number of failures (Hossain et al., 2018)	28
Figure 2-10 Reliability characteristics for different components of wind turbine (Faulstich et al., 2011)	29
Figure 2-11 classification of joints (DNVGL-RP-C203).....	31
Figure 2-12 SCF of T joint (DNVGL-RP-C203).....	32
Figure 2-13 stress concentration in T joint (Tong et al., 2019)	32
Figure 2-14 Definition of geometrical parameters (DNVGL-RP-C203).....	33
Figure 3-1 density functions with different mean and standard deviation.....	37
Figure 3-2 Log-Normal distributions with a different mean and standard deviation	38
Figure 3-3 FORM approximation of the failure surface (Maier et al., 2001).....	39
Figure 3-4 reliability-based design curve (Melchers, 2018).....	41
Figure 3-5 Basic R-S problem (Melchers, R.E., 2018).....	41
Figure 3-6 $x^2 - 3x + 2$	43
Figure 3-7 summing the rectangles (Cumer et al. 2020)	44
Figure 4-1 Weibull distribution	47
Figure 4-2 Damage curve.....	48
Figure 4-3 gaussian and exponential kernel plot (Rasmussen and Williams, 2006)	50
Figure 4-4 Gaussian Process distribution	51

Figure 5-1 lognormal distribution.....	54
Figure 5-2 integrating lognormal with deterministic damage.....	54
Figure 5-3 Gaussian Distribution with noise included	56
Figure 5-4 Gaussian Distribution without noise	56
Figure 5-5 Damage Curve starting with 5 points.....	57
Figure 5-6 Damage Curve after adding a point	57
Figure 5-7 Damage Curve with 65 observations and length scale of 1.0	58
Figure 5-8 No. of observations vs length scale.....	58
Figure 5-9 The length scale vs the standard deviation with having a constant number of points	59
Figure 5-10 the relation between the length scale and the failure probability with having 65 data points.....	59
Figure 5-11 Gaussian Process with 0.05 noise and 100 data points	62
Figure 5-12 Gaussian Process with 0.05 noise and 200 data points	63
Figure 5-13 Gaussian Process with 0.02 noise and 100 data points	63
Figure 5-14 Relation between the noise and standard deviation with having 100 data points.....	64
Figure 5-15 Relation between the standard deviation and the no. of points with having a constant noise of 0.05.....	64
Figure 5-16 the relation between the noise and reliability with having 100 data points	65
Figure 5-17 the relation between no. of points and the probability of failure with having constant noise of 0.05.....	65
Figure 6-1 Gaussian distribution with different length scales	67
Figure 6-2 convergence of the failure probability	68

List of Tables

Table 2-1 Surface roughness in different terrains.....	23
Table 5-1 Total damage comparison.....	53
Table 6-1 Comparison between the different methods of obtaining the probability of failure	69

Chapter 1: Introduction

1.1 Wind Turbines

Wind turbines have been considered as one of the primary power sources in the renewable industry. They are used onshore and offshore, and both have a considerable contribution in generating the required energy for residential and economic purposes. The industry is now heading towards offshore wind turbines. It allows more power to be generated due to the wind profile's higher wind speeds and stability during the different seasons of the year. Offshore wind turbines enable the industry to go more prominent in both the generation capacity and turbine size. The offshore wind turbines reached 8-10 MW in use today, with 12-15 MW being under development.

One of the most critical issues to be handled is wind turbines' safety and their substructures; as the development tends towards larger wind turbines, the failure frequency increases[1]. Wind turbines face multiple failure modes such as Gearbox failure modes, Generator failure modes, and Rotor blade failure modes.

There are multiple approaches to estimate the loads due to waves and wind acting on the substructure and the turbine. A practical method is to evaluate the loads using simulations of different load cases and different environmental conditions. A fatigue analysis is an essential procedure that leads to knowing the lifetime of each member of the structure. A statistical model is then evaluating the probability of failure of different members of the structure.

In this thesis, the issue of calculating the fatigue life of an offshore wind turbine jacket is to be addressed and discussed. The goal is to calculate the fatigue reliability of an offshore wind turbine (OWT) jacket by using statistical models. For accuracy, time-domain analysis of the load and response is needed. However, this is rather time-consuming. Hence, for efficient analysis of the lifetime of integrated offshore wind turbine models, the load case assessment is simplified. The load-response simulations of the fixed jacket are typically implemented using OpenFAST software for the different load cases and environmental conditions. The results obtained from these time simulations are, by the use of rain-flow counting procedures, used to estimate load cycles and the fatigue damage.

A practical approach is to simulate the load cases, and the outcome data can be used as test data. These data can then be used to build the approximation model. A more general way uses

probability distributions with only a few parameters to estimate the fatigue load, which allows for quick but not too accurate estimates.

The accuracy depends on the data used for estimating the parameters; the studies mentioned above relied on many hundred load cases in the time domain to achieve acceptable accuracy. It is not clear how this methodology can efficiently estimate fatigue damage when the design of the structures is changed.

As a new approach, we present a more efficient method for simplified fatigue load assessment. We focus on the estimation of the total fatigue damage of the structure. The main idea is that a few selected load cases are sufficient for estimating the real fatigue damage.

The calculation of structural reliability is implemented via simulating the model using different load cases and load case combinations. The load cases are reaching hundreds of load case combinations. However, we need a few numbers of those combinations, and to find the most reliable data, we have to use statistical modelling.

1.2 Motivation and Objective

The motivation for this thesis is based on developing an efficient approach for determining the fatigue reliability that may lead to a cost-efficient design for offshore substructures. The main objective is to use probabilistic models to estimate the reliability of the structure with a low number of data points as possible. The accuracy of results increases with increasing the number of points. Nevertheless, sub-objectives have to be done as a predecessor to the main objective throughout the thesis. Research has to be done for literature review and results from previously tested approaches of simplified analysis.

1.3 Approach

The structural reliability of the addressed jacket is estimated using the OC4 jacket structure. The model is assessed using finite element methods as a time-domain simulation in OpenFAST, calculating all forces and moments acting on each structure member. Furthermore, calculations for fatigue damage and estimation of the reliability will be done using Julia's programming language.

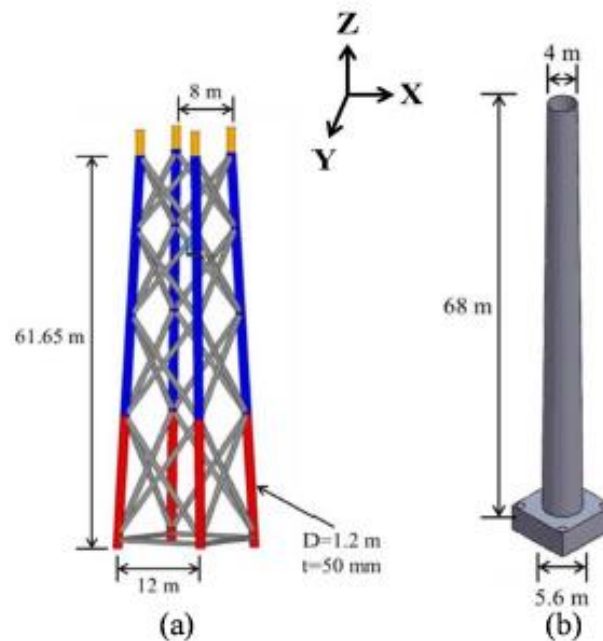


Figure 1-1 OC4 Jacket substructure CAD model(a), and simplified tower model(b) (Lai et al., 2016)

Structural reliability analysis will be estimated by performing probabilistic analysis and distributions with OC4 model structure. Other parameters affecting the loads on the structure, such as Aerodynamic damping and member stiffness, are included in the input files of OpenFAST and their results in the output files and represented in detail.

The steps of calculating the reliability are as follows:

- Using OpenFAST to simulate wind conditions and a sea state based on given wave height, wave period, and wind speed.
- Reading the output file in Julia to import loads of the members and using them for the fatigue load estimation.
- Identifying the type of the structure's joints and estimate the stress concentration factor (SCF) for each joint type using DNVGL-RP-C203 for fatigue design.

- Using the calculated SCFs to estimate the hot spot stresses.
- Using the Rainflow counting method to estimate the fatigue cycles within a time domain.
- Using the outcome from the rainflow counting to obtain the fatigue damage through a simulation of 60 minutes.
- Using the resulting damage curve along with probability densities of the same wind speeds using Weibull distribution.
- Implementing different methods to calculate the probability of failure of the structure and having the numerical solution as the reference value.
- Estimating the reliability from the results obtained from the previous methods.
- Using a meta-model, Gaussian Process, as a new approach to estimate the reliability of the OC4 jacket.
- Choosing the training data points to be used in the meta-model and developing the best method of selecting these training observations.
- Comparing the results from the Gaussian Process with the reference value to check the accuracy of the method.

The damage curve is extracted from a pre-performed analysis of the OC4 model. The model is assessed in a time-domain simulation. This curve was extracted to implement the deterministic damage methods (MCI, Bins method, and numerical integration) and obtain the probability of failure. The Gaussian process is using the Weibull distribution and indicating how the damage curve should look like, as the curve is unknown.

In this thesis, the last seven points are implemented, starting with using Weibull distribution and the damage curves and ending with comparing the results obtained from the Gaussian Process with the other methods. The Gaussian process regression uses the Weibull distribution.

1.4 Structure of the thesis

- Chapter 2 presenting a background about wind energy and the calculation of loads caused by environmental conditions.
- Chapter 3 presents a better understanding of the thesis. It includes the finite elements and approaches used before and the progress up to date, and how is the probabilistic modelling is of use along the reliability estimation process.
- Chapter 4 explains the used methodology and detailed approach steps and how the used approach stands compared to the currently used techniques.
- Chapter 5, the calculations and results of the models and simulations are presented.
- Chapter 6 presents the discussion of the obtained results and how these results are improving the methods of reliability estimation
- Chapter 7 is presenting the conclusion of the previously shown results and the suggested further work.

Chapter 2: Background

2.1 Offshore wind turbine

Although offshore wind turbines have a high cost, some advantages compensate for this issue. The higher wind speeds produce magnificently higher power per unit capacity. Offshore wind turbines also complement solar photovoltaic (PV) as it produces efficiently in winter as the load becomes at its peak day in and day out throughout the year.

Offshore wind farms began operating in the 1990s. Specifically, the world's first wind farm started running in 1991 in Vindeby, featuring 0.45 MW turbines. Looking at the wind farms now, they have more than 14 GW of cumulative installed capacity worldwide[2].

Substructures for offshore wind turbines are humongous, weighing over 1000 tons for wind turbines of 5 MW.

The substructures of wind turbines are categorized as fixed and floating substructures. In this thesis, we address the OC4 jacket. OC4 jacket is a fixed substructure that is still in the theoretical phase, designed but not implemented yet in practice.

2.2 Fixed substructures

The used offshore substructure in this study is the fixed piled structures, primarily used in shallow water; these structures are widely known as jacket structures. More than 90% of the offshore platforms existing now are using jacket structure. This type of fixed substructure is a tubular structure fixed to the seabed by drilled and grouted piles. The water depth for the jacket structure does not exceed 500m [3], [4].

The types of fixed substructures are:

- Monopile
- Jacket
- Tripod
- Gravity based

Scour can be a problem facing all types of fixed substructures, depending on water depth (WD), soil type, grading, and seabed current.

It might be allowed to develop even longer piles or gravel and rock dump protection required (costs around €500 -700 k per monopile). Alternatives include frond mats, the so-called plastic seaweed, rock mats, pile eddy breaking fin or diversion berms, and fences[5].

In offshore structures, failure is caused mainly by insufficient pile strength. The phenomena of scouring have a significant effect on the load transition and the pile strength[6]. The necessity of considering scouring phenomena amplifies when the scour depth becomes remarkable, which can endanger the jacket stability.

The main thing that should be put into consideration is the loads caused by wind and waves. Wave loads and wind speeds cause many load cases, and the forces acting on the turbine tower can be calculated using Morison's equation.

Morison's equation calculates the wave force applied to a body by a uniform unsteady flow

$$D(t) = \frac{1}{2} C_D A \rho U(t) |U(t)| + C_M V \rho \frac{dU(t)}{dt} \quad 2-1$$

Where

V, A: Volume and cross-section area of the body

C_D : drag coefficient

$C_M = c_m + 1$: inertia force coefficient, where "1" accounts for a hydrostatic force component in the accelerated fluid.

With assuming having a regular wave, we can use an Airy wave which is a sinusoidal wave.

Airy wave's wave elevation can be determined as:

$$\eta(x, t) = \frac{H}{2} \cos(kx - \omega t) = \frac{H}{2} \text{Re}\{e^{i(kx - \omega t)}\} \quad 2-2$$

And the velocity potential:

$$\phi = \frac{\frac{gH}{2\omega} \cosh[k(z + d)]}{\cosh(kd)} \cos(kx - \omega t) \quad 2-3$$

Dispersion relation:

$$c^2 = \frac{\omega^2}{k^2} = \frac{g}{k} \tanh(kd) \quad 2-4$$

Where

$$\omega^2 = gk * \tanh(kd) \quad 2-5$$

As we are dealing with a fixed bottom wind turbine so using a jacket is recommended, and jackets are built in shallow water, and this is known when $d < \frac{\lambda}{20}$ then the frequency can be calculated as:

$$\omega^2 = gk * kd \quad 2-6$$

As in shallow water $kd \ll 1$ so we can consider $\tanh(kd) \approx kd$

Two essential factors that affect the calculation of the wave loads are acceleration and velocity.

Acceleration:

$$\frac{\partial u}{\partial t}(x, z, t) = a\omega^2 \frac{\cosh(k(h+z))}{\sinh(kh)} \cos(\omega t - kx) \quad 2-7$$

$$\frac{\partial w}{\partial t}(x, z, t) = -a\omega^2 \frac{\sinh(k(h+z))}{\sinh(kh)} \sin(\omega t - kx) \quad 2-8$$

Velocity:

$$u(x, z, t) = a\omega \frac{\cosh(k(h+z))}{\sinh(kh)} \sin(\omega t - kx) \quad 2-9$$

$$w(x, z, t) = a\omega \frac{\sinh(k(h+z))}{\sinh(kh)} \cos(\omega t - kx) \quad 2-10$$

For the wind, it is different compared to the onshore wind. Offshore wind changes uniformly as it is stable mainly during springtime and mostly unstable during wintertime. On onshore, the current changes diurnally. This significant difference is that the sea surface has a vast area. It saves the temperature, high heat capacity for a long time, leading to small temperature changes advancing through time [7], [8].

Also, offshore we deal with non-stationary lower boundary, ocean waves, which depends on the wind speed.

The lower surface roughness offshore results in a very different vertical structure of the boundary layer, i.e., the depth of the surface layer can be as low as 30m [9].

For the non-stationary boundary layer, we have different wind profile for different wind speeds

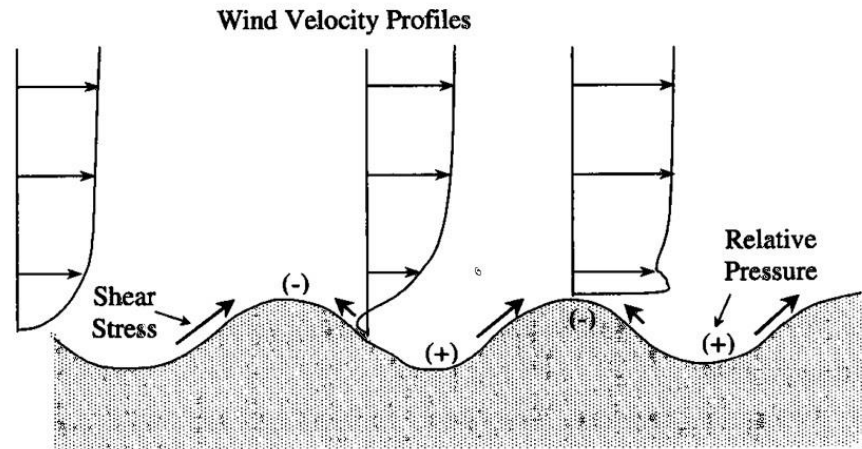


Figure 2-1 wind profile (Halici and Mutungi, 2016)

The jacket structure is best suitable for shallow water and intermediate water up to 500 m depth. In shallow water, the waves are long, and as waves move closer to surface water, the phase velocity decreases. The wave amplitude increases, and the waves start bending, breaking, and making a significant impact on the structure, causing a substantial load on the jacket's leg and members.

2.3 Power law wind profile

The relation between the wind speeds at a certain height and another is known as the wind profile power law.

$$U(z) = u_{ref} \left(\frac{z}{Z_{ref}} \right)^\alpha \quad 2-11$$

Where U is the wind speed at the hub height Z and u_{ref} is the wind speed at the reference hub height Z_{ref} . α is the power-law exponent that is a coefficient derived empirically that differs depending on the atmospheric stability. A commonly used value of α is 0.143 in neutral stability conditions[10], [11].

This method is currently recommended in IEC standards, but this profile does not have a fundamental physical basis and is only valid for neutral wind conditions.

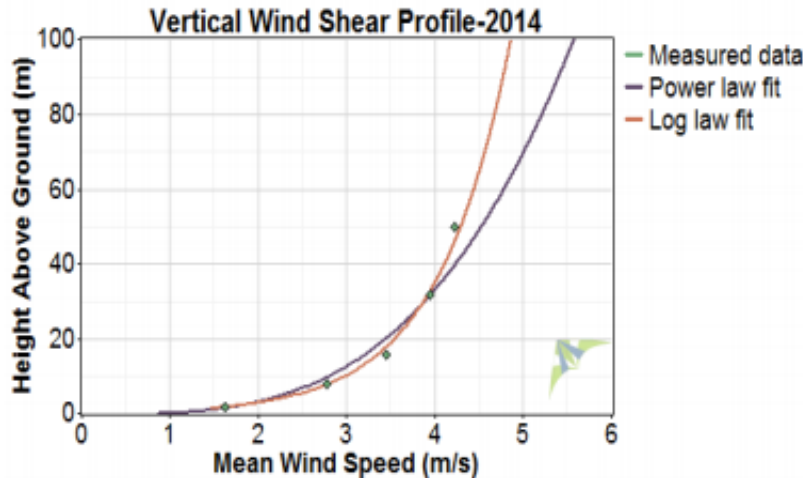


Figure 2-2 vertical wind shear profile (Maran, Sard 2019)

2.4 Logarithmic wind profile

The log wind profile is a commonly used semi-empirical relationship to define the vertical distribution within the lowest boundary layer of the horizontal mean wind speed.

The wind speeds logarithmic profile is available within the first 100 m, the so-called surface layer, of the atmosphere. The rest of the atmospheric layer, up to 1000 m, is composed boundary layer and the free atmosphere.

$$U(Z) = \left(\frac{u_*}{k}\right) \left(\ln \frac{Z}{Z_0} - \varphi\right) \quad 2-12$$

Where $k = 0.4$ refers to Von Karman's constant, z is the height, u_* is the friction velocity, z_0 is the surface roughness length, and φ is a stability-dependent function.

A corrective measure to rely on for the effect of the surface roughness of a wind flow is the roughness length.

It is challenging to define absolute values because of the indication of the values range by references.

This method is currently recommended on the DNV standards and is based on Similarity theory. In most cases, the roughness length z_0 is given based on specific terrain descriptions.

Table 2-1 Surface roughness in different terrains

Terrain	k_r	Z_0	Z_{min} EN 1991-4	Z_{min} Nat. Annex
Sea or coastal area exposed to the open sea.	0.155	0.003	1	2
Rough open sea, lakes with at least 5 km fetch upwind and smooth flat country without obstacles	0.17	0.01	1	2
Farmland with boundary hedges, occasional small farm structures, houses, and trees	0.19	0.05	2	4
Suburban or industrial areas and permanent forests	0.22	0.3	5	8
Urban areas in which at least 15% of the surface is covered with buildings and their average height exceeds 15m	0.24	1	10	16

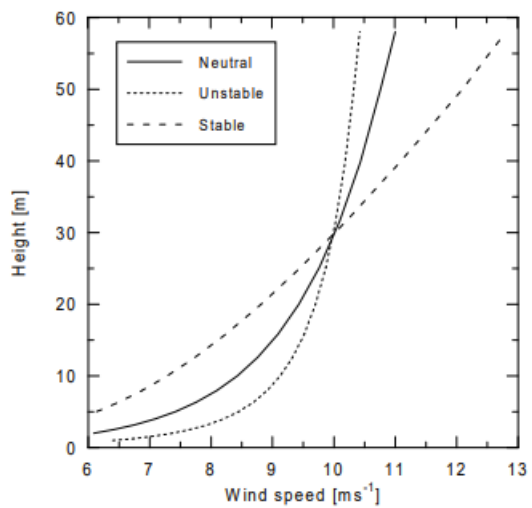


Figure 2-3 wind speed profiles vs static stability in the surface layer (Abdalla et al., 2017)

The profiles shown in Figure 2-3 are matched at 30 m, but the roughness length of them all is the same. The difference in the mean wind gradient is caused by the different instabilities, although they are for the same terrain and hub height.

Different pressure and temperature gradients with height can cause different stability conditions. An example of such an effect on the wind profile is shown in Figure 2-4 below [12].

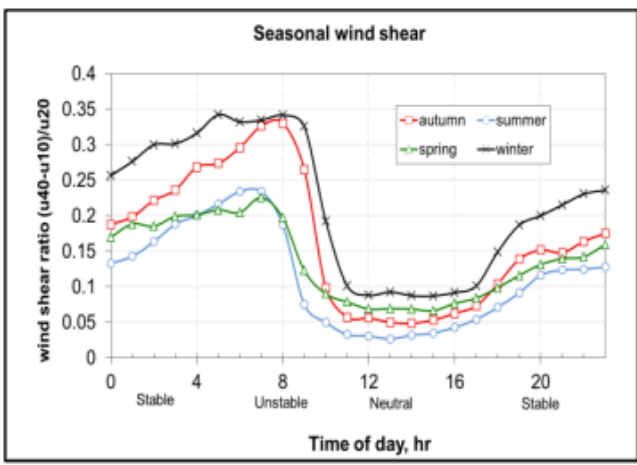


Figure 2-4 seasonal cycle of wind shear (Abdalla et al., 2017)

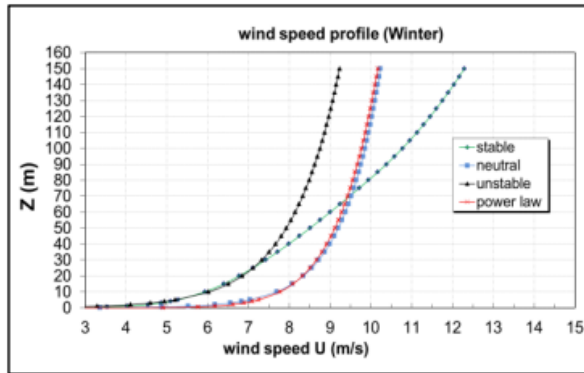


Figure 2-8 Wind speed profiles for different conditions in Winter (Abdalla et al. (2017))

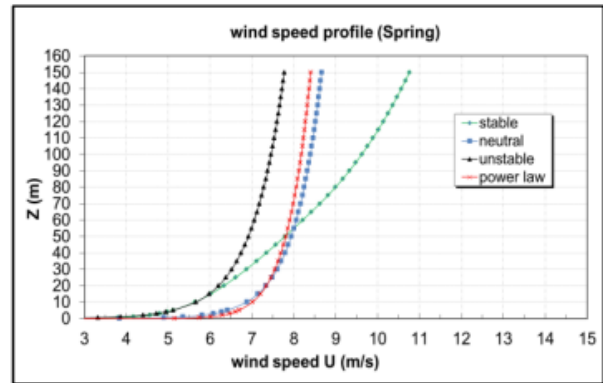


Figure 2-7 Wind speed profiles for different conditions in Spring (Abdalla et al. (2017))

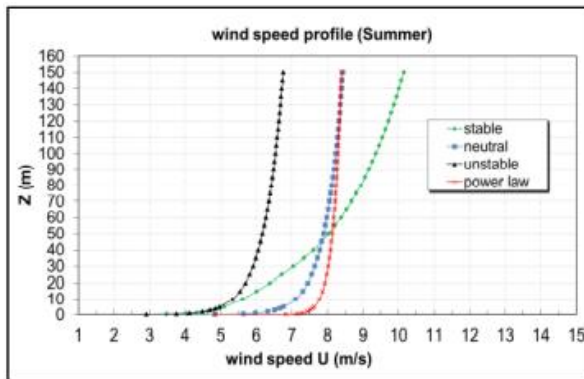


Figure 2-5 Wind speed profiles for different conditions in Summer (Abdalla et al. (2017))

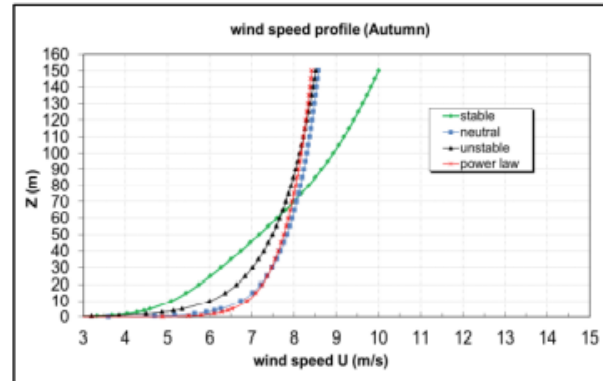


Figure 2-6 Wind speed profiles for different conditions in Autumn (Abdalla et al. (2017))

Experimentally obtained (mean) wind forces on different objects/cross-sections are commonly expressed in terms of non-dimensional force coefficients, which depend on the cross-section shape and, in some cases, also on Reynolds number.

C_D : drag coefficient expresses the static force in the along-wind direction, $F_D \equiv D$ normalized with the velocity pressure and the cross-sectional height H , i.e., the wind-exposed area $H \times 1$ m:

$$C_D = \frac{F_D}{\frac{1}{2} \rho U^2 H} \quad 2-13$$

C_L : lift coefficient expresses the mean force in the across-wind direction, $F_L \equiv L$ normalized with the velocity pressure and the "lift-generating area" B ($B \times 1$ m).

$$C_L = \frac{F_L}{\frac{1}{2}\rho U^2 B} \quad 2-14$$

The resulting aerodynamic load does not necessarily act at the shear center of the cross-section, i.e., it may also generate an overturning moment.

CM: moment coefficient expresses the mean overturning moment M about the shear center, L normalized with the velocity pressure and the "lift-generating area" B times arm reference value B , i.e., B^2 ($B^2 \times 1\text{m}$).

$$C_M = \frac{M}{\frac{1}{2}\rho U^2 B^2} \quad 2-15$$

Force coefficients are typically obtained either by direct force measurements or by integrating the surface pressures, i.e., surface pressure coefficients C_p , Where

$$C_p = \frac{p - p_0}{\frac{1}{2}\rho U^2} \quad 2-16$$

p and p_0 are local pressure referenced to the static pressure and normalized by the velocity pressure.

2.5 Mean and total wind load

The dynamic pressure acting on a structure associated with wind speed U is defined as:

$$q = \frac{1}{2}\rho U^2 \quad 2-17$$

Comprehends the force on a wind-exposed structural area A using a shape factor C_A :

$$F_q = C_A A q \quad 2-18$$

We can also calculate the force per unit length by replacing the exposed area with a reference dimension $D/B/H$.

The shape factor reflects the integrated effect of mean surface pressures on the structural cross-section/wind-exposed area as the airflow passes the structures.

Turbulence is an inseparable part of wind flow, so the total wind load includes a time-varying, fluctuating component, in addition to the mean value:

Where:

$$F_{tot} = C_A A \frac{1}{2} \rho U_{tot}^2 \quad 2-19$$

$$U_{tot}^2 = (U + u)^2 \quad 2-20$$

In the case of a "small", "point-like" structure, i.e., a structure small compared to the size of significant eddies in the natural wind, the largest total force on the structure can be formulated:

$$F_{max} = F_q + k_p \sigma_F = F_q (1 + k_p 2I_u) \quad 2-21$$

Where σ_F is the standard deviation of the load, which depends on the turbulence intensity I_u : $\sigma_F = F_q 2I_u$ and k_p is the peak factor, which relates the maximum variation of the force to its standard deviation. For a normally distributed process k_p is in the range from 3-5. More significant peak factors may be present in the suction regions around the building corners or on the roof of a building.

Equation 2-21 gives the most significant force expected on a point-like structure, i.e., a structure small compared to the size of substantial eddies in the natural wind.

In the case of a "large" structure, the above expression modifies into:

$$F_{max} = F_q (1 + k_p 2I_u \sqrt{k_b}) \quad 2-22$$

Where, k_b is a factor taking into account the lack of turbulence over the structural span or surface.

2.6 Mal functions of components

The downtimes calculated are due to both regular maintenance and unexpected malfunctions. The following evaluations refer only to the unexpected malfunctions, which concerned half mechanical and half electrical components[13].

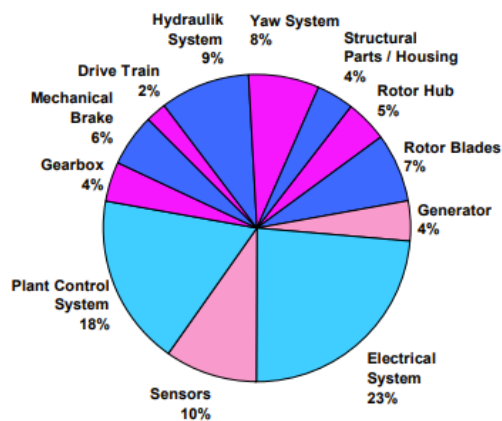


Figure 2-9 main components' share of the total number of failures
(Hossain et al., 2018)

Regardless of failure rates, downtimes of machines after a failure are an essential factor in defining a machine's reliability. Downtime duration caused by malfunctions is dependent on necessary maintenance and repair work, replacement parts availability, and the personnel capacity of service teams. Previously, generator repairs, drive train, hub, gearbox, and blades have usually caused hold periods of several weeks [14].

Considering all the reported repair measures that are available now, the average rate of failure and downtime per component can be given. It is noticed that the downtimes declined in the past five to ten years. So, the high number of failures of some components is now balanced out to a certain extent by short standstill periods. However, damages to generators, gearboxes, and drive trains are mainly caused by extended downtime of one week as an average [15], [16].

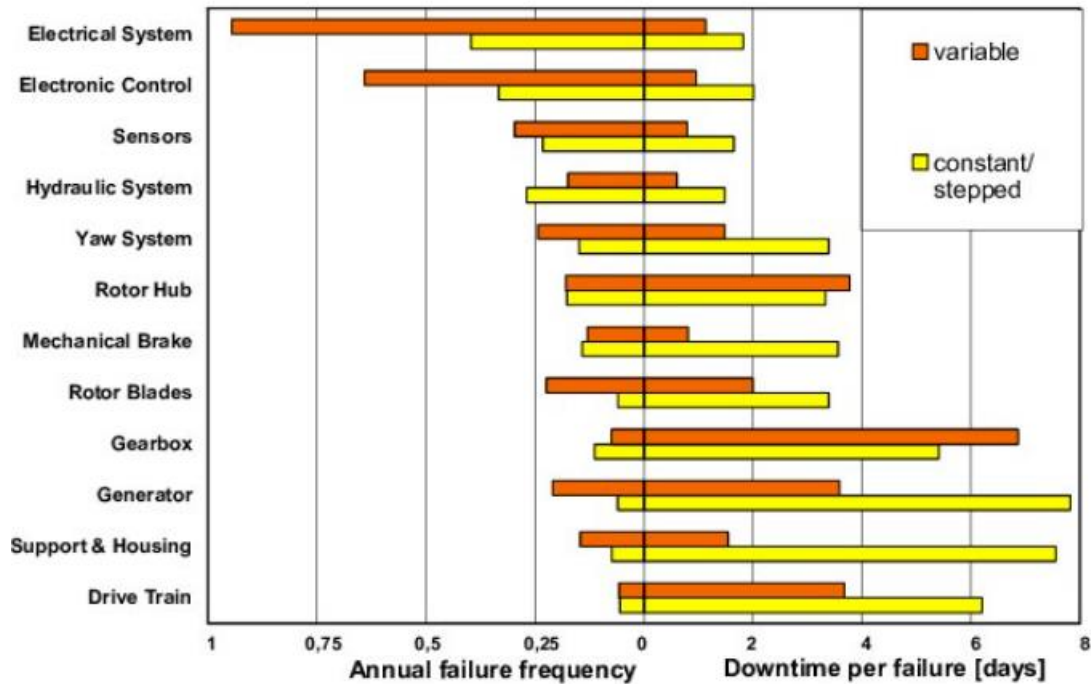


Figure 2-10 Reliability characteristics for different components of wind turbine (Faulstich et al., 2011)

The industry-accepted turbine lifetime is 20 years. Thus, a wind turbine's reliability is the percentage of time that the turbine will be functioning at total capacity during appropriate wind conditions at a site with specified wind resource characterization for a 20-year life. Reliability specialists use a graphical representation called the bathtub curve. The bathtub curve consists of three regions; an infant mortality period with a decreasing failure rate followed by an average life period with a low and relatively constant failure rate and ending with displaying an increasing failure rate of the wear-out period[17], [18].

2.7 Fatigue Analysis

The primary failure focused on in this thesis is fatigue failure. Fatigue is the most common type of failure an offshore structure experiences due to the different and cyclic environmental loads applied by the wind and waves. Defining the type of joints is required to understand the fatigue

subjected to the OC4 jacket, as there are different types of joints such as T, X, Y, K, and complex joints.

In the DNV-RP-C203 standard for fatigue design, different types of fatigue modes and joints types are mentioned. As the jacket addressed is made of tubular joints, the nominal stress can be calculated using the simple beam theory as:

$$\sigma_{Nominal} = \frac{P}{A} \pm \frac{M}{I} y \quad 2-23$$

Where P is the applied axial load, A is the cross-sectional area, M is the applied bending moment, I is the inertia of the section area about the neutral axis, and y is the perpendicular distance from the neutral axis to a point on the section. [19]

The intriguing matter is what defines the axial load. The most probable guess is that the x-axis is where the axial load exists, to make sure this is the right guess, the local axis has to be transformed into the correct coordinate to define the direction of every load in x y and z. This transformation can be done by multiplying the transpose of the transformation matrix by the load vector[20]. After estimating the nominal stresses, we need to calculate the fatigue damage, which is defined in DNV standard as it is dependent on the S-N curve and is estimated as:

$$D = \sum_{i=1}^k \frac{n_i}{N_i} = \frac{1}{\bar{a}} \sum_{i=1}^k n_i \cdot (\Delta\sigma_i)^m \quad 2-24$$

Where

D = accumulated fatigue damage

\bar{a} = intercept of the design S-N curve with the log N axis

m = negative inverse slope of the S-N curve

k = number of stress blocks

n_i = number of stress cycles in stress block i

N_i = number of cycles to failure at constant stress range $\Delta\sigma_i$

As shown in the equation, stress is the hot spot stress, and the hot spot stress is the stress that we are most interested in. The hot spot stress is simply calculated by multiplying the nominal stress by a stress concentration factor (SCF). Defining the type of the joints depend on the direction of the forces and moments, if the load is compression or tension, and if the moment is in-plane or out of plane. Having the global to local transformation matrices from the output files, the definition of the in-plane and out of plane became more accessible as we can assume a coordinate system of local x, y, and z and then use the inverse of the global to local transfer matrices and then transforming from the global back to the assumed coordinate system.

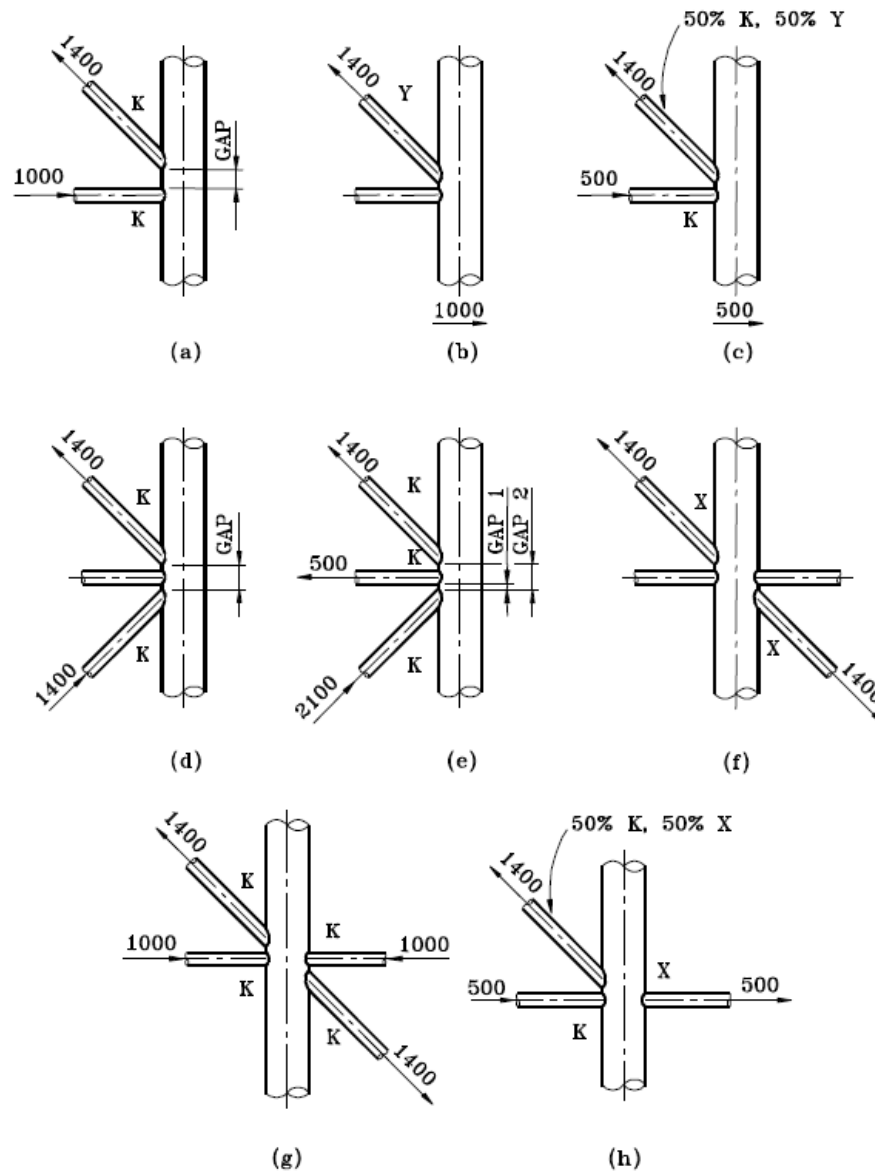


Figure 2-11 classification of joints (DNVGL-RP-C203)

A complex joint is defined as a joint that has a combination of Y and K, or X and K joints properties. Geometrical parameters play a significant role in calculating the SCF of each joint. So, taking a simple T joint, for example, as shown below in Figure 2-12, with in-plane bending, SCF is calculated as

For chord crown:

$$1.45\beta\tau^{0.85}\gamma^{1-0.68\beta}(\sin\theta)^{0.7}$$

For brace crown:

$$1 + 0.65\beta\tau^{0.4}\gamma^{1.09-0.77\beta}(\sin\theta)^{0.06\gamma-1.16}$$

Where β is the ratio between the brace diameter and the chord diameter, τ is the ratio between the thickness of the brace and thickness of the chord, γ is $\frac{D}{2T}$, θ is the angle between the brace and the chord.

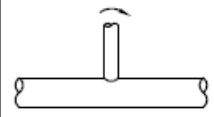
<p>In-plane bending</p> 	<p>Chord crown:</p> $1.45\beta\tau^{0.85}\gamma^{1-0.68\beta}(\sin\theta)^{0.7}$
	<p>Brace crown:</p> $1 + 0.65\beta\tau^{0.4}\gamma^{1.09-0.77\beta}(\sin\theta)^{0.06\gamma-1.16}$

Figure 2-12 SCF of T joint (DNVGL-RP-C203)

To further explain the stress concentration phenomena in the T joint discussed above, the zone of

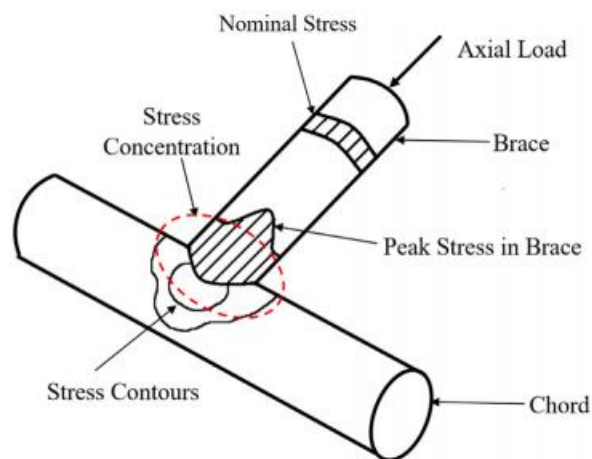


Figure 2-13 stress concentration in T joint (Tong et al., 2019)

the stress concentration is pointed at in Figure 2-13 above[16].

As shown in Figure 2-13, it is clear that the stress at the welded joint is higher than the nominal stress due to the stress concentration.

The main goal is to calculate the damage done to the joint due to environmental conditions. Calculating the nominal stress is the main procedure for calculating the damage.

However, the stress we are interested in is the hot spot stress, and that is calculated by multiplying the SCF by the nominal stress calculated.

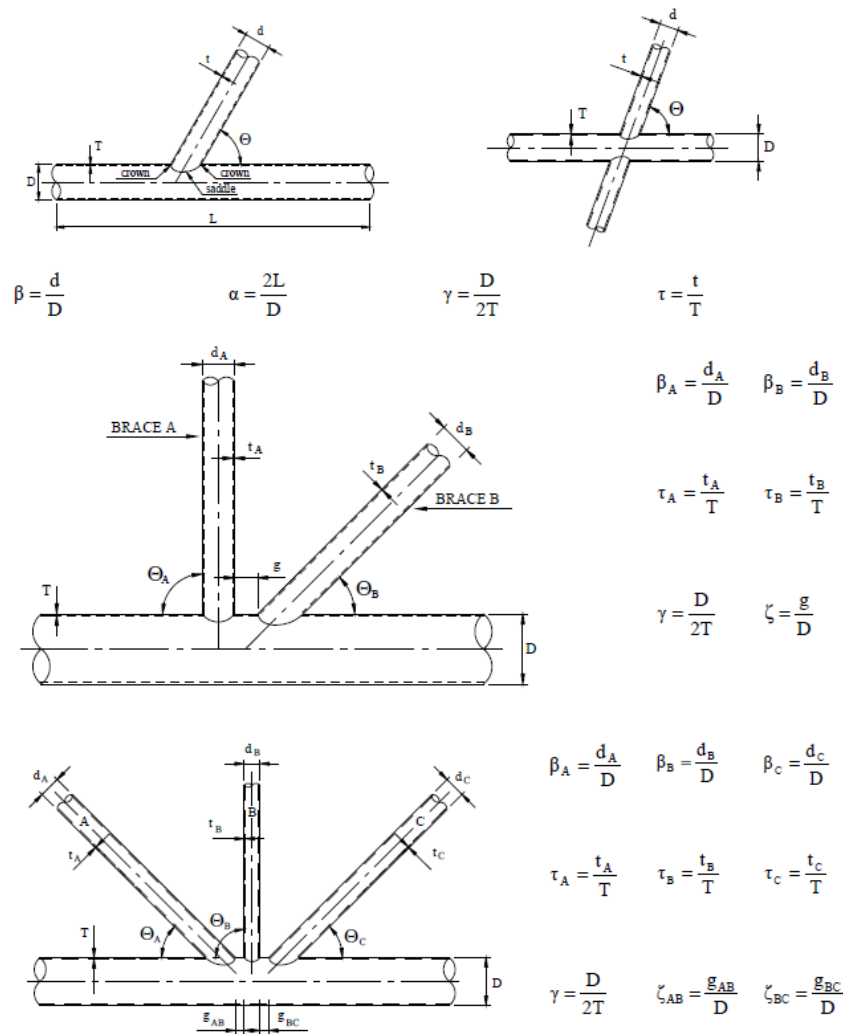


Figure 2-14 Definition of geometrical parameters (DNVGL-RP-C203)

To analyze the design, a simplified numerical procedure is implemented to reduce the demand for large fine-mesh models for the calculation of SCF factors:

- the stress concentration or the notch factor due to the weld itself is included in the S-N curve to be used, the D-curve. This S-N curve is also known as the hot spot S-N curve.

- The stress concentration due to the geometric effect of the precise detail can be calculated using different methods, such as considering the use of solid elements, resulting in a geometric SCF factor.

This procedure is defined as the hot spot method.

The hot-spot stress method, which is also known as the geometric stress method, considers the stress increment effect due to the structural discontinuity except for the stress concentration due to weld toe, i.e., without the consideration of the localized weld notch stress. Hot spot stress is the value of the structural stress of the surface at hot spots. The hot spots are located at a welded joint where the cracks possibly initiate under cyclic loading due to the increased stress value.

In the hot spot stress method, the fatigue life is related to hot spot stress directly instead of the nominal stress. The fatigue life of tubular and non-tubular joints is usually identified using $S-N$ curves. An $S-N$ curve shows the relation between the hot spot stress range and the number of cycles to failure. The performance fatigue life of tubular and non-tubular joints is also dependent on the structural members' thickness. The fatigue life of tubular and non-tubular joints gets decreased as the thickness of the structural member increases.

Chapter 3: Literature Review

The offshore wind industry faces many challenges in the support structures design process, and the main challenge would be the cost of design. The main goal of reliability analysis is to have an optimal design with a lower cost. When we address fatigue damage assessment, we often discuss the fatigue load of an offshore wind turbine in time-domain simulations, which leads to a long process. To obtain a high level of accuracy in the results, we use a large number of load cases, and the objective to be achieved here is reaching an accurate solution with a lower number of load cases. There are many approaches applied to achieve this goal using statistical models.

3.1 Modelling of uncertainties in structural engineering

Close to all input parameters in a structural design problem is associated with uncertainties, which need to be addressed in the analysis. As an example, the load on a turbine has uncertainties due to the randomness of the environmental conditions, such as the wind speed. Furthermore, it is associated with uncertainty in, for example, the drag coefficient (C_d). In addition, there are uncertainties in system parameters, such as the damping coefficient and the stiffness of the soil.

The modelling of these uncertainties is a crucial point within the formulation of a structural problem of offshore wind turbines. There are several mathematical and statistical models to describe these uncertainties in a probabilistic model of the structure.

A probability distribution is a statistical function. The function describes the likelihoods that a random variable can obtain in a range of given numbers. The probability distribution functions are typically described by their mean, standard deviation, kurtosis, and skewness.

The normal distribution is the most common. The normal distribution is frequently used in Engineering, investing, finance, and science. The normal distribution is defined and characterized by its mean and standard deviation, which means that the distribution is neither skewed nor exhibits kurtosis, which makes the distribution symmetric.

To the probability of occurrence of uncertain events which are naturally stochastic, two main functions are used, and those are the probability density function and cumulative density function.

To describe a random variable statistically, it can be entirely described by using a cumulative density function as $F_X(x)$ or by using a probability density function $f_X(x)$, shown as follows

$$F_X(x) = P(X \leq x) = \int_{-\infty}^x f_X(x) dx \quad 3-1$$

The distribution of the variables is defined by some parameters in association with the probability distribution. These parameters are known as statistical moments. Known that the most commonly used moments are the mean value $\mu(X)$, known as the first moment, and also called the expected value as denoted by $E(X)$, and the second moment, known as variance and denoted by $\sigma^2(X)$ or $\text{Var}(X)$. the two moments (parameters) can be described as follows:

$$\text{Mean: } \mu(X) = \frac{\sum_{i=1}^N X_i}{N} \quad 3-2$$

$$\text{variance: } \sigma^2(X) = \frac{\sum (x - \mu)^2}{N} \quad 3-3$$

The probability distributions used for structural engineering are log-normal, uniform, and Weibull distributions. A significant parameter in the distributions is the coefficient of variation (CV), and it is defined as the standard deviation divided by the mean value[21].

$$CV = \frac{\sigma}{\mu} \quad 3-4$$

A very common continuous distribution presenting the probability is the normal or Gaussian distribution. One can define the density function of such probability distribution by plotting a curve with specific mean and standard deviation as follows:

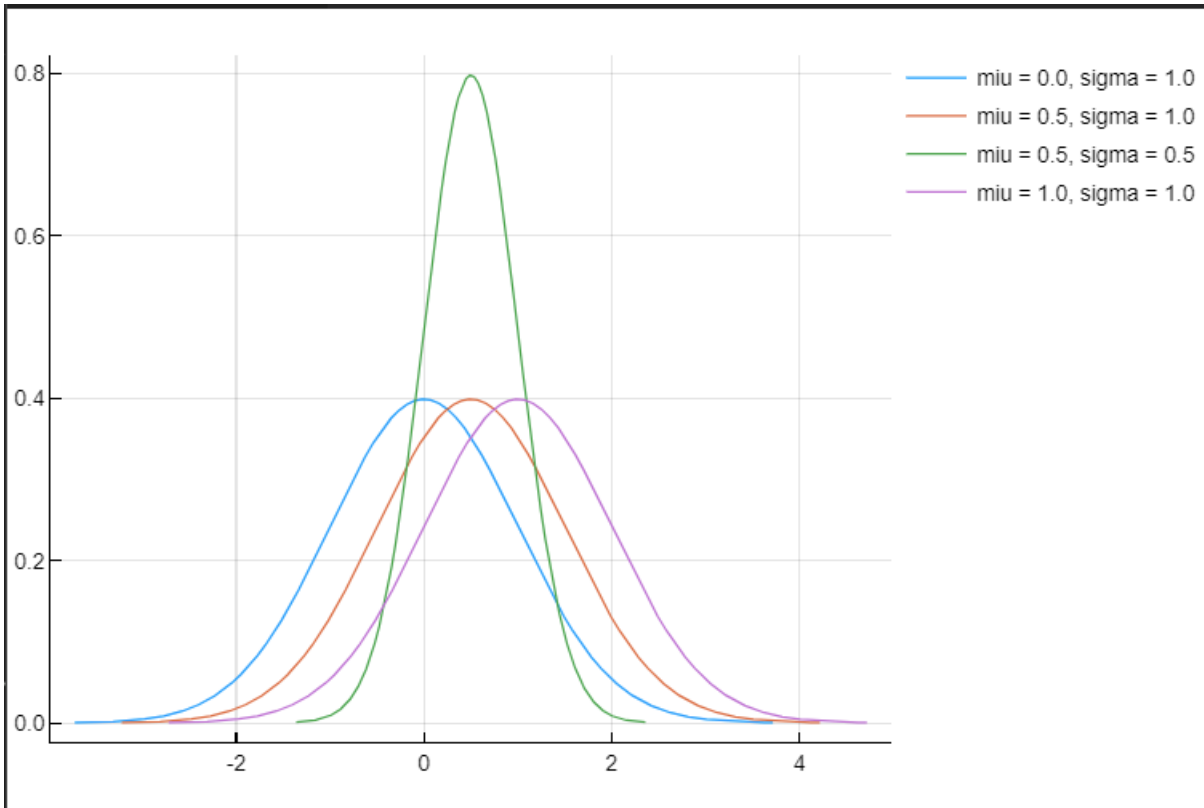


Figure 3-1 density functions with different mean and standard deviation

$$f(x; \mu, \sigma) = \frac{1}{\sigma\sqrt{2\pi}} e^{-\frac{(x-\mu)^2}{2\sigma^2}} = \frac{1}{\sigma} \varphi\left(\frac{(x-\mu)}{\sigma}\right) \quad 3-5$$

Where

$$\varphi(x) = \frac{1}{\sqrt{2\pi}} e^{-\frac{1}{2}x^2} \quad 3-6$$

Another type of continuous probability distribution is the log-normal distribution. The log-normal distribution has random variables that possess a logarithm that is normally distributed.

To plot a distribution with specific mean $\mu(x)$ and variance $\sigma^2(x)$ we can use

$$\mu = \ln\left(\frac{\mu^2(X)}{\sqrt{\mu^2(X) + \sigma^2(X)}}\right) \quad 3-7$$

$$\sigma^2 = \ln\left(1 + \frac{\sigma^2(X)}{\mu^2(X)}\right) \quad 3-8$$

And both of those variables are positive. The probability distribution has a density function defined as follows

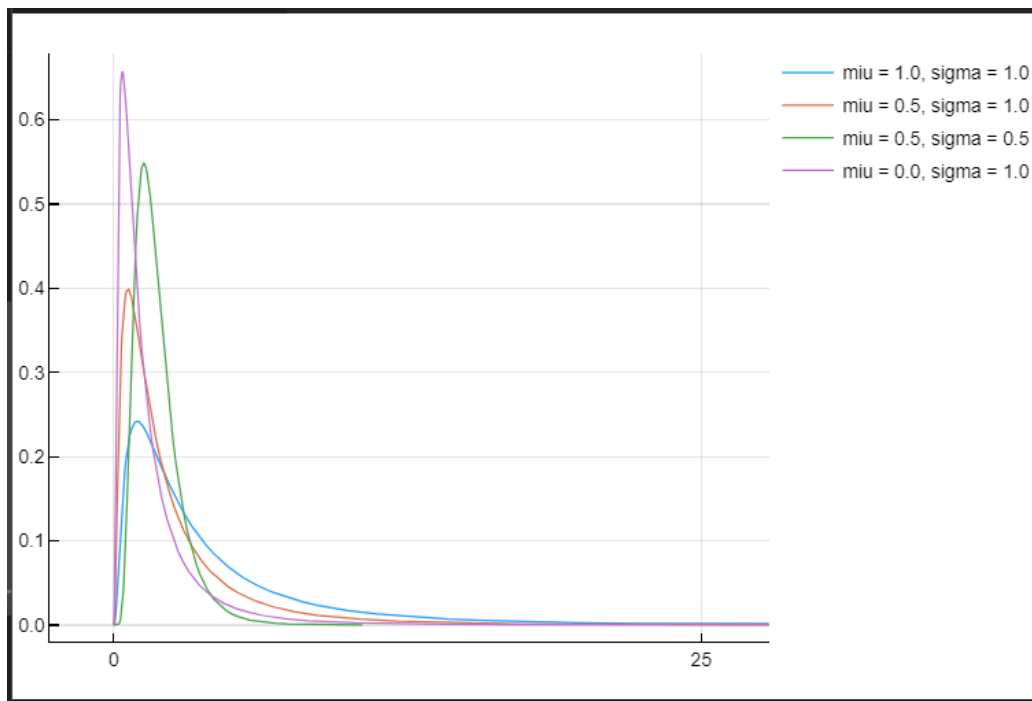


Figure 3-2 Log-Normal distributions with a different mean and standard deviation

3.2 First-Order Reliability Method (FORM)

FORM was developed originally to assess the structures' reliability [22], [23]. The objective of FORM is to estimate the integral in 3-9 and hence the failure probability.

$$P_f = \int_{G(X) < 0} f_x(X) dx \quad 3-9$$

Where $G(X) = R - L$; R is resistance and L is load, and $f_x(X)$ is the probability density function of X.

The failure probability is obtained by using the computed reliability index β as

$$P_f = \Phi(-\beta)$$

Where Φ is the normal cumulative density function. If we have n random variables, β is then defined as the minimum distance between n variable mean and the failure surface as shown in Figure 3-3 below [24].

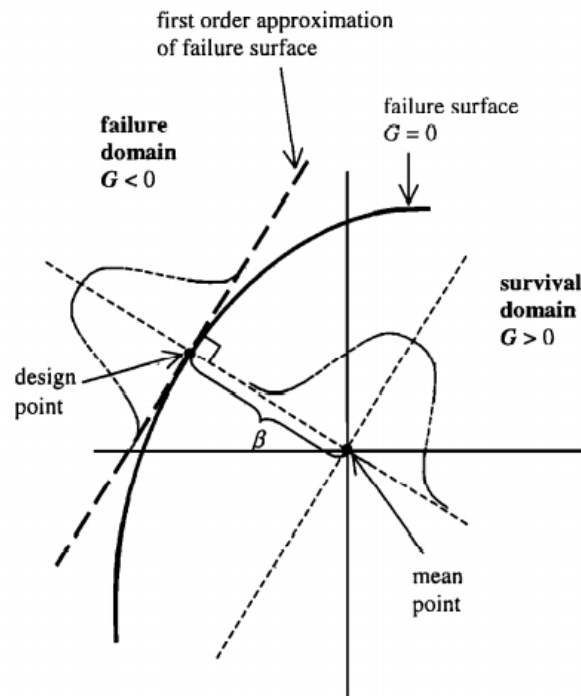


Figure 3-3 FORM approximation of the failure surface (Maier et al., 2001)

3.3 First-Order Second-Moment (FOSM) method

The FOSM, also known as mean value first-order second-moment (MVFOSM) method, in probability theory is a method to determine the moments of a function that has random input variables[25]. The FOSM method is an approximation methods, and one of the most commonly applied in engineering. The method took the name from the fact that it uses the first-order term of the Taylor series expansion about the mean value of each input variable and requires up to the second-moment of the uncertain variables. Furthermore, it allows the estimation of uncertainty in the output variables without knowing the shape of the probability density functions (PDFs) of input variables in detail. The mean value and the standard deviations of the input variables suffice to compute the mean value and standard deviation of the output. For a better understanding of the principle of this method, we consider a function y transforming a random variable X into random variable Y , where $Y = y(X)$. The expected mean value can be estimated as

$$E(Y) = \int_{-\infty}^{\infty} y(x)p_X(x)dx \quad 3-11$$

And the variance is

$$Var(Y) = \int_{-\infty}^{\infty} [y(x) - E(Y)]^2 p_X(x) dx \quad 3-12$$

Where p_X is the PDF of X . The mean and variance of Y require information of p_X , which in many cases the available information is limited to the mean and variance of X . Furthermore, even knowing p_X , the computation of the integrals in Equations 3-11 and 3-12 may, to a great extent, consume time (Ang & Tang, 1975) [26].

3.4 Structural Reliability Analysis

The goal is to determine how reliable these structures are, using a statistical model that reduces uncertainties in the estimates of the probability of failure of the jacket.

Structural reliability is capable of including uncertainties in the parameters of a structural system and the different environmental loads.

A deterministic approach to structural engineering is typically based on the partial factor, and limit state method, also called the Load and Resistance Factor Design (LRFD). This method addresses uncertainties in parameters by determining the characteristic values of material properties and load intensities. In addition, partial safety factors are used to cope with some aspects of uncertainty. However, it might not in all cases be cost-optimal and may in some cases be too much on the safe side. Hence, for offshore wind turbines, it is of interest to investigate methods such as structural reliability analysis in order to seek a more cost-efficient design.

A suitable way of obtaining this, probability of failure, the risk is the approach of probabilistic models. Such an approach allows designing the structure with a sufficient and acceptable probability of failure during the structure's lifetime.

The simplest problem of structural reliability is illustrating this theory. If we consider a single load effect S that is resisted by a single resistance R . each of these parameters is defined by a known probability density function, f_S and f_R respectively, expressing both R and S in the same unit, as illustrated in Figure 3-4.

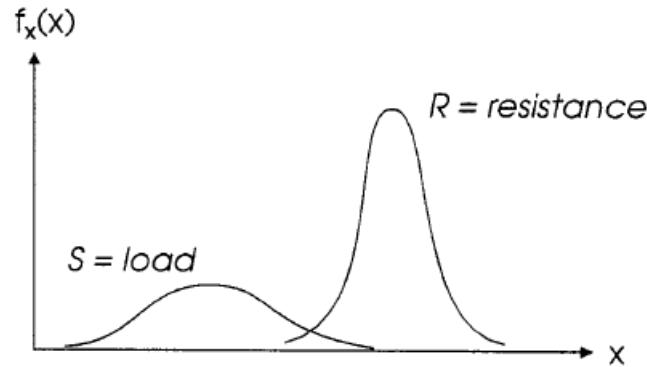


Figure 3-4 reliability-based design curve (Melchers, 2018)

The failure of the structure in this simple example can be considered to occur if the resultant S is surpassing the resistance R . The probability of failure of an element can be defined as follows [27], [28].

$$p_f = P(g(R, S) \leq 0)$$

3-13

Where g is the limit state, and the failure probability is the same as the probability of violating the limit state. Equation 3-13 can be used to estimate the probability failure of a probabilistic model for the number of observations considered in the analysis. A reliability analysis is required for the statistical description of the limit state values $g_i (i = 1, 2, 3, \dots, n)$. Defining the statistical characteristics using the most suitable probability distributions is an essential step before implementing reliability analysis. Eventually, the probability of failure is estimated using numerical calculations efficiently and economically.

This is known as “convolution integral”, with meaning easily explained as shown in Figure 3-5.

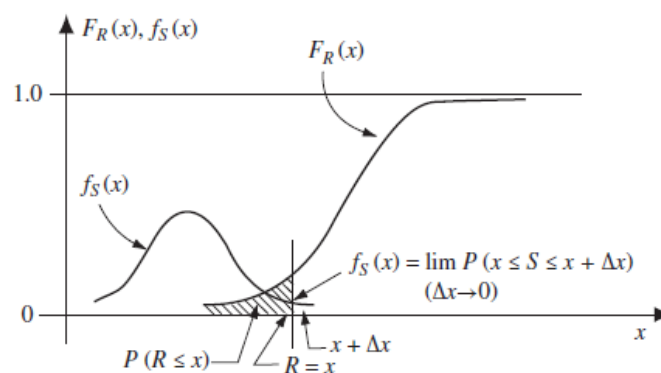


Figure 3-5 Basic R-S problem (Melchers, R.E., 2018)

$F_R(x)$ is the probability that $R \leq x$ or the probability that actual resistance R of the member is less than range value x . This failure is represented if the loading is larger than x . The probability of this case is given by the term $f_S(x)$ that represents the probability of the load effect S that acts in the member has a value between x and $x + \Delta x$ in the limit as Δx goes towards zero. By considering all possible values of x , i.e. by taking the integral over all x , the total failure probability is obtained.

$$P_f = \int_{-\infty}^{\infty} (1 - F_S(x)) f_R(x) dx \quad 3-14$$

This can be defined as the summation of the failure probabilities of the load that exceeds the resistance.

Numerous methods have been developed aiming to obtain the integrated probability in structural reliability analysis. The most common methods are the first and second-order reliability methods (FORM and SORM) and Monte Carlo simulation. Direct methods to integrate over the failure domain is also in use by different numerical integrating methods, such as the Newton-Raphson method, Monte Carlo Integration and the so-called Bins method. These approaches aimed to estimate the failure probability from the data provided by the test of many samples and data points[29], [30].

The term Structural reliability of a structure refers to the probability of safe performance of a limit state. Limit states refer to ultimate failures, such as collapse, or unserviceability, such as deflection, vibrations, or crack propagation. An efficient way to designing a structure is using a probabilistic model to treat structural loads and resistance. Structural reliability is becoming the ideal way of designing a structure as it replaces the deterministic traditional ways of maintenance and design.

The reliability can be estimated as

$$Reliability = 1 - P_{failure}$$

The reliability-based design has the objective of ensuring that the failure probability of a system is reasonably low.

3.5 Bins Method

The bins method, or as known Numerical Binning, is a method to group or collect a number of more or fewer values which are continuous into smaller bins number. Creating bins or ranges helps

in understanding the numerical data in a better way. Taking, an example, data on the age of a group of people, we might want to have their ages arranged into a smaller number of age intervals.

The same thing can be illustrated in the data collected to calculate the reliability of a structure from having the damage of every wind speed ranging from 0 to 40m/s. Arranging this wind speed range into smaller groups, 5m/s for example, helps in understanding the data sets better than taking the whole range at once[31].

3.6 Monte Carlo Integration

The numerical integration in mathematics uses equally spaced numbers in calculations. The difference between Monte Carlo Integration and numerical integration is the use of random numbers.

A simple way to illustrate this method is integrating a univariant function s denoting by S the integral value

$$S = \int_a^b s(x)dx$$

This integral can be considered as the area below the curve of the function. Taking a random function as

$$s(x) = x^2 - 3x + 2$$

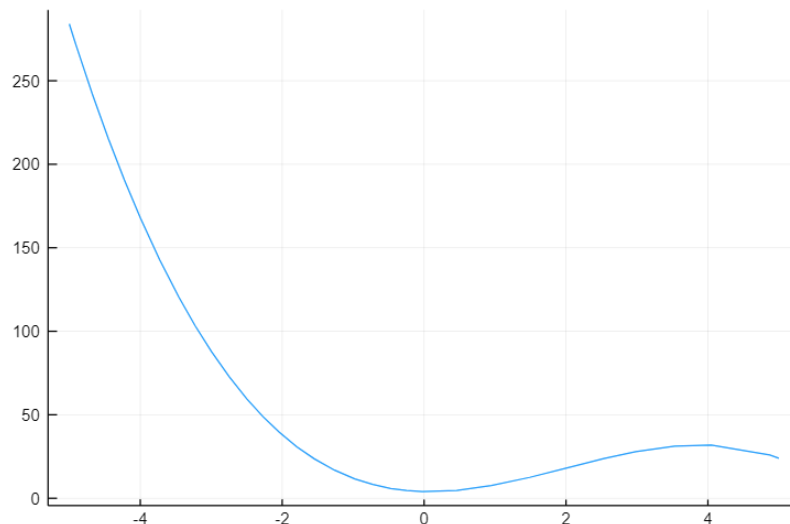


Figure 3-6 $x^2 - 3x + 2$

The function can be plotted as shown in Figure 3-6 above and choosing $a = -2$ and $b = 5$

If we choose a random x value between a and b , multiplying $s(x)$ by $(b - a)$, we get the area of a rectangle width of $b - a$ and the height of x . The main reason why Monte Carlo is to estimate an approximation of the integral value by the average area of the rectangles shown in Figure 3-7 below, computed for random chosen x values [32].

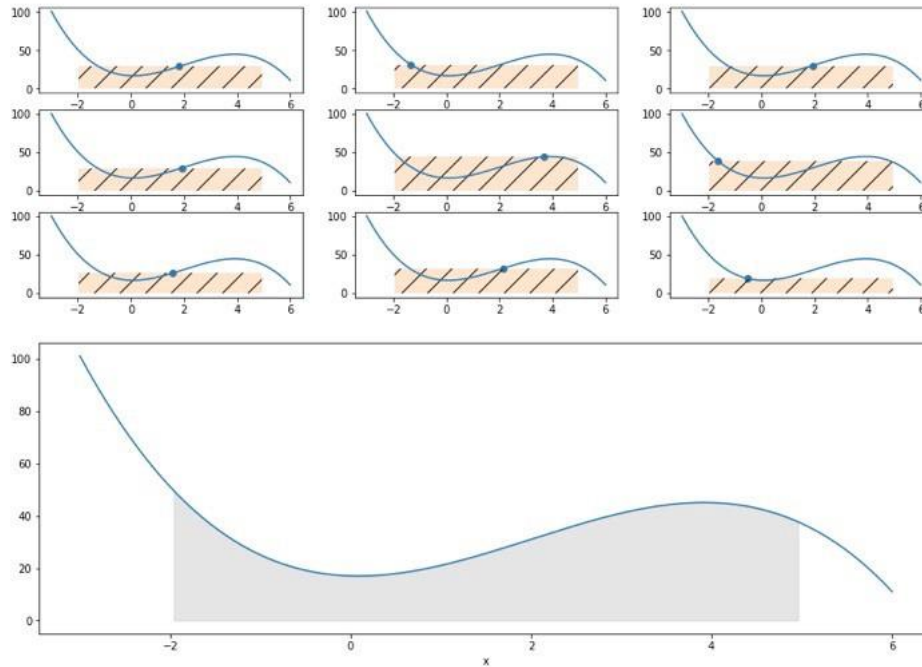


Figure 3-7 summing the rectangles (Cumer et al. 2020)

By summing the area of the rectangles and obtaining the average of the sum, the number keeps getting closer to the actual result of the integral. The idea is generally formalized as

$$F^N = (b - a) \frac{1}{N - 1} \sum_{i=0}^N f(X_i)$$

Where X_i is the random variable chosen for every rectangle. Large numbers have a law that gives us that as N tends to infinity, the true value of the integral becomes:

$$P_r(\lim_{N \rightarrow \infty} (F^N) = F) = 1$$

That means that the more numbers are used in this method, the more accurate the results become.

The Monte Carlo method has been used before for reliability estimation with some limitations of simplifying the structure. This method showed relatively well performance, managing to assess

structural reliability with doable effort. The results obtained by this approach is indicating the importance of the probabilistic assessment in the optimization of a structure's design [33].

3.7 Numerical Integration

The numerical integration method is computing an approximation to the integral of a certain function. In structural reliability, numerical integration can be used for obtaining the failure probability in a high accuracy manner. The use of this method starts with combining the probabilities with the required parameter to be assessed and integrate them numerically.

Numerical integration is still used to estimate structural reliability, and it showed higher accuracy than the traditional first-order second-moment method (FOSM). When a small number of points is used, it shows lower accuracy yet satisfying to the accuracy requirement in engineering. With a higher number of points, the accuracy increases accordingly[34], [35].

3.8 Gaussian Process

The Gaussian Process is a stochastic process with random variables defined by time and space, and every collection of those variables has a multivariate normal distribution. The process allows predicting the available data by incorporating previous knowledge. It is commonly used in fitting a function of the data, which is basically called regression.

The Gaussian process as a tool is powerful in machine learning. It is not limited to regression but can also be used in classification tasks. Each data set has infinitely many functions to help with fitting the data. The Gaussian process gives a creative and elegant solution to this problem by simply assigning probabilities to every function. Additionally, the use of probabilistic approaches allows us to include the confidence of the regression results from the prediction[36].

The model can then predict the mean and variance of function value at new points. The main Gaussian process is defined as

$$f(x) \sim GP(m(x), k(x, x'))$$

Where $m(x)$ is the mean function and $k(x, x')$ is the kernel function. The mean function gives the mean at any point of the input space, and the kernel sets the covariance between points. Usually, the mean is set to zero for simplicity, and the kernel should be positive definite[37].

A Gaussian process regression (GPR) defines a probabilistic model over a set of given data points. It is constructed so that the probability of the value of the function is maximized for all given data points. The process is successfully used in many fields such as Internet of Things (IoT), prediction analysis of time series, and dynamic system control[38]–[40]. GPR method, however, continues to possess a few deficiencies such as calculations and limitation of the noise distribution. Studies revealed that selecting the hyperparameters significantly affect the GPR performance. The optimal selection of these hyperparameters leads to significant reduction of iterations of GPR learning and improve the accuracy of model fitting. Optimizing the parameters can be done using experiment trials and experience selection. However, these types of optimizing methods involve deficiencies, including the high cost of calculation and poor efficiency[41]. In this thesis, the GPR is implemented in Julia, where two optimization methods: conjugate gradient and L-BFGS.

Conjugate gradient (CG) is a solver which is iterative, used for linear equation systems $Ax = b$ where $A \in \mathbb{R}^{N \times N}$ a real, positive definite, and symmetric matrix. In practice, CG is used as an approximate solver, and it can provide a good estimation to x in significantly small N steps[42].

The Broyden-Fletcher-Goldfarb-Shanno (BFGS) is an iterative method for solving unconstrained nonlinear optimization problems. Furthermore, L-BFGS is using a limited amount of computer memory. It is a typical algorithm for parameter estimation in machine learning. This algorithm's target problem is to minimize $f(x)$ over unconstrained values of the real vector x where f is a differential scalar function.

The use of the Gaussian process in structural reliability in previous studies showed promising results with the process managing to significantly reduce the number of required training data points and providing accurate estimations of the failure probability when compared to the FORM[43], [44].

Chapter 4: Methodology

The methodology of this thesis objectives is the approach of using statistical modelling to obtain the fatigue reliability of the jacket structure. The industry uses methods that are time-consuming and costly, implementing the different numerical approaches with deterministic damage values to compare between them and the applied approach, statistical model, of the Gaussian Process. The comparison will show how the statistical approach is standing against the currently used methods in terms of accuracy and time efficiency.

The Gaussian process is defined by its mean and covariance functions, where the mean function $m(x)$ describes the mean of any point in the process, and the kernel $k(x, x') = \sigma^2$ describes the covariance between two training points.

The Gaussian process is a non-parametric model. That makes it easier as we do not have to worry about fitting too much data, training, points added to the model, unlike a linear model on a non-linear data point.

4.1 Wind Distribution

The wind speed probability is in the thesis modelled by a Weibull distribution.

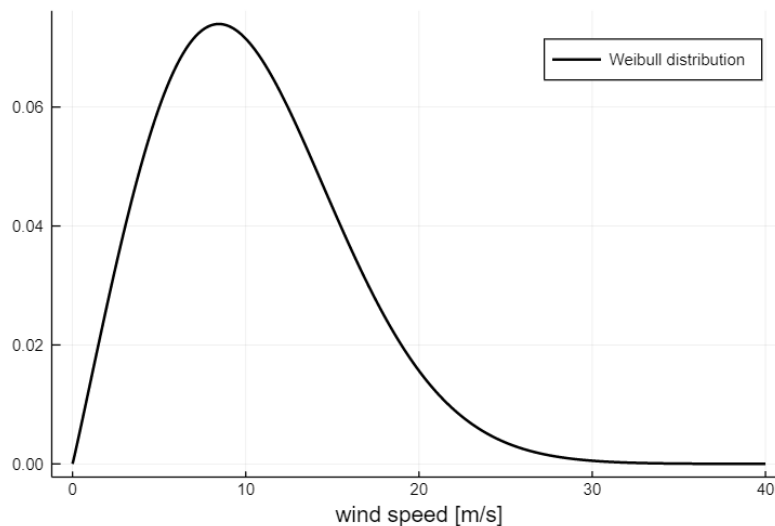


Figure 4-1 Weibull distribution

4.2 Damage Curve

The damage curve used in this thesis is extracted from the results obtained from the research article “Simplified fatigue load assessment in offshore wind turbine structural analysis” written by Daniel Zwick and Michael Muskulus [45]. For each member connected to a Y-joint, K-joint or X-joint, FEDEM Windpower was used to establish the time series data for the axial force as well as in-plane and out-of-plane bending moments as outputs. From the raw time series data, a transient of 60 to 200 seconds was cut off depending on the wind speed. The simulation produced results in a total analysis length of 60 minutes. Force and moment time series were converted to sectional stresses, using beam cross-section data for the specific members. Using Equation 2-24, these time series are adjusted by the relevant SCF, and then a rainflow counting method is used in order to get the n and $\Delta\sigma$. With these and the relevant $S - N$ curve, the total damage is calculated.

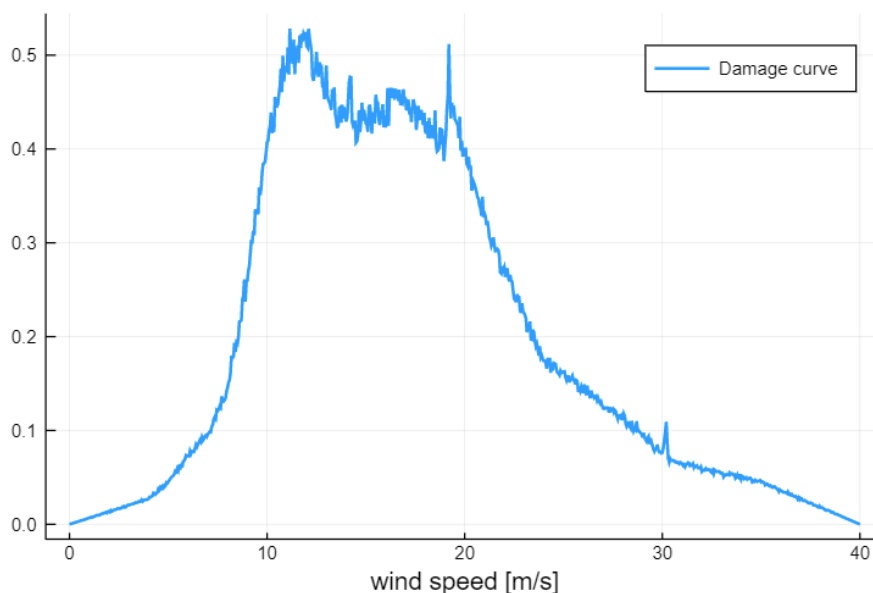


Figure 4-2 Damage curve

4.3 Total damage estimation

The results of the damage and the probability density function corresponding to wind speed are obtained for the jacket.

The total damage required to estimate the reliability is obtained using four methods:

- Damage estimation using numerical integration
- Damage estimation using bins method

- Damage estimation using Monte Carlo Integration (MCI)
- Damage estimation using Gaussian Process

4.3.1 Numerical Integration

This method demands combining the damage curve with the probability density distribution and then integrating them numerically at every damage position for every wind speed. The results obtained from numerical integration are considered, in this thesis, as the reference results.

4.3.2 Bins Method

This method is implemented by obtaining the probabilities by integrating the probability densities at every wind speed and then multiplying these probabilities with every damage corresponding to the same wind speeds.

4.3.3 Monte Carlo Integration

In numerical integration, the used methods are using a deterministic approach in obtaining the total damage. However, Monte Carlo integration utilizes a non-deterministic approach. Each set of chosen points give a different outcome as they are chosen randomly. The outcome is an approximation of the true value or the reference value of the total damage, which is the numerical integration, value with respective error bars. These error bars are likely to contain the reference value or the required accurate value.

This method is implemented with the same procedure as the Bins method in having the probabilities estimated and then combining each probability with the corresponding damage.

4.3.4 Failure probability using deterministic value

The total damage estimated using the three previously explained methods is used to obtain the failure probability by integrating the PDF of the normal distribution of $\mu = 1$ and $\sigma = 0.3$ with the total damage. This integral can be described as shown in Figure 5-2 in Chapter 5:.

4.3.5 Gaussian Process

The Gaussian Process still possesses high uncertainty in controlling the distribution using its length scale and standard deviation. In Julia, the used package "GaussianProcess" requires four inputs: training data in X and Y, the kernel, and the gaussian mean. The Gaussian process is mainly controlled by its mean and kernel. The kernel is dependent on two variables: the length scale and standard deviation. The used type of kernel in this thesis is the squared exponential kernel, and it can be described as shown in Figure 4-3 below

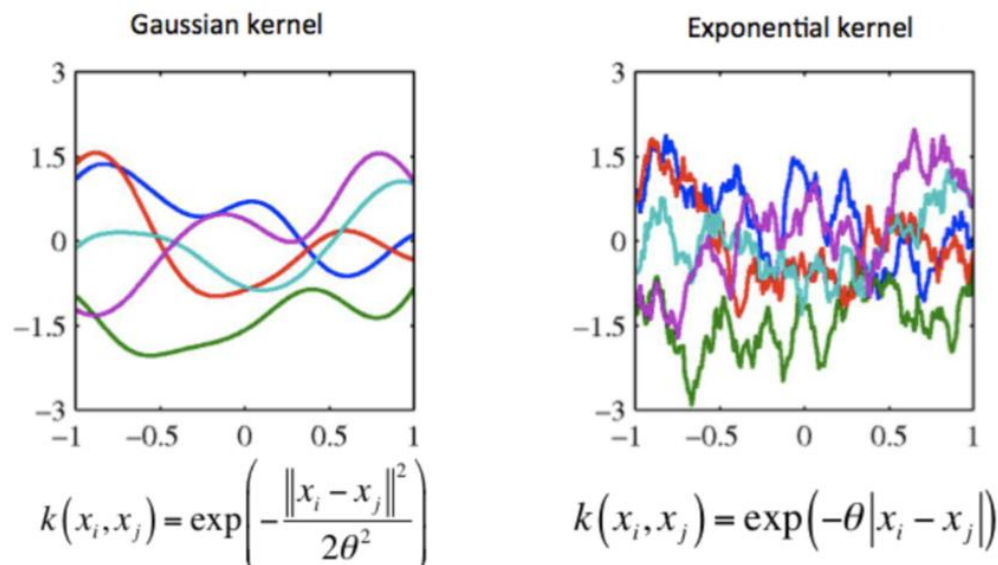


Figure 4-3 gaussian and exponential kernel plot (Rasmussen and Williams, 2006)

Controlling the kernel is implemented by fixing a mean with a zero value and changing the kernel accordingly by choosing the data points.

After plotting the gaussian distribution, the mean curve values and the variance are obtained using a prediction function in the "GaussianProcess" package. Then the mean and the covariance matrix are calculated using those predicted data generated.

The probability of failure is estimated by integrating CDF of the log-normal of a mean value of 1.0 and a standard deviation of 0.3 with the PDF of the normal distribution of the Gaussian Process's mean and standard deviation, as shown in Equation 3-14.

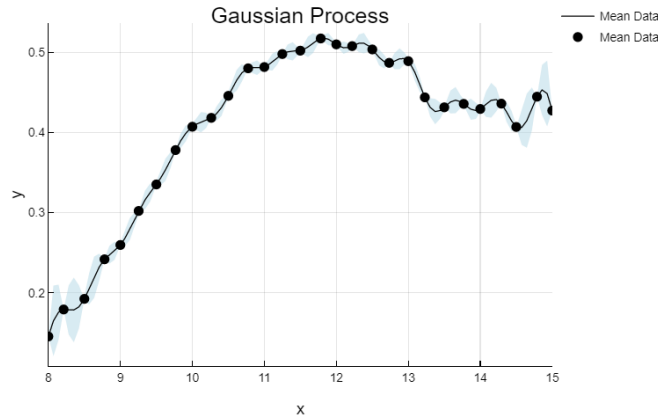


Figure 4-4 Gaussian Process distribution

The reliability can be obtained by simply using the equation $Reliability = 1 - P_f$. The procedure of the proposed method is as follows:

1. Assuming initial data points $R = (R_1, R_2, R_3, \dots, R_n)$.
2. Building the training datasets and scale them.
3. Train the Gaussian process model through the training datasets and obtain the optimum hyperparameters required. The kernel used in this thesis is the squared exponential.
4. Extract the explicit formulation of the approximate performance function through the use of the well-trained GP model.
5. Compute the failure probability of the Gaussian process.
6. Check the convergence criterion for $(P_f(i) - P_f(i - 1)) < 0.0001$.
 - a. If the criteria are not satisfied, then repeat step 3 to step 6 until they are satisfied.
 - b. If the convergence criterion is satisfied, then implement the next step.
7. Calculate the structural reliability.

Chapter 5: Results

5.1 Damage Estimation

The total damage is estimated using both the probability densities from the Weibull distribution and the damage distribution.

5.1.1 Damage Estimation Using Bins Method

As explained before in the Bins method, the process requires estimating the probabilities by integrating the probability densities with the wind speeds.

- Using $N = 7$, we get a damage of 0.2558089937513546
- Using $N = 100$, we get a damage of 0.2758387314741845
- Using $N = 500$, we get a damage of 0.2738720963063552

As shown from the results above, the more bins we use, the more accurate the results are. Reaching a high number of samples shows results very close to the reference value with a difference of almost 0.0001%.

5.1.2 Damage Estimation Using Monte Carlo Integration

The difference between Monte Carlo Integration and the Bins method is that Monte Carlo chooses random points to evaluate the damage. In contrast, the Bins method chooses specific points to evaluate the damage.

- Using an "Rn" value of 100, we get a damage value of 0.25726065445676505
- Using an "Rn" value of 10000, we get a damage value of 0.2737818225936027
- Using an "Rn" value of 1000000, we get a damage value of 0.2738712725766772

As we can observe from the above-shown results, the more points we used, the closer we get to the reference value of the numerical integration. Using 1000000 showing a difference of almost 0.0004% between Monte Carlo damage and the reference damage.

5.1.3 Damage Estimation Using Numerical Integration

Numerical Integration is different from the two previous methods. The probability densities and the damage distribution are combined first before Integrating the resultant array with the wind speeds.

The resulting damage in using $S = 0.004$, which is 10000 points, is 0.27387240804147867.

Usually, the industry uses a step length of 1m/s, and in that case, we get resulting damage of 0.2738724080351072.

The total damage obtained from the Numerical Integration using 100,000 data points is

$$\text{Total Damage} = 0.27382$$

5.1.4 Method Used in the Industry

In practice, the used method is choosing a point for every wind speed. Having a wind speed varying from 0 to 40m/s makes them have 40 data points.

5.2 Damage Comparison

Using the Bins method for each wind speed gives results as follows

$$\text{Total damage} = 0.27317$$

That brings us to the comparison between these results, as shown in Table 5-1 below

Table 5-1 Total damage comparison

	Bins Method	Monte Carlo Integration	Numerical Integration	Method in Practice
Total Damage	0.2738720963063552	0.2738712725766772	0.27382	0.27317
Difference compared to reference value	0.019%	0.018%	-	0.24%

5.3 Reliability estimation

Estimating the reliability using the load resistance method in deterministic values is done by integrating the lognormal curve with the damage resulting from the methods above. The normal distribution, in this case, has a mean of 1 and a CV of 0.3. the lognormal parameters can be calculated as follows:

$$\text{Mean} = \exp\left(\mu + \frac{\sigma^2}{2}\right) = 1$$

$$\text{Variance} = [\exp(\sigma^2) - 1] \exp(2\mu + \sigma^2) = 0.3$$

So, $\mu = -0.0431$ and $\sigma = 0.2935$

The lognormal is then integrated with the deterministic damage estimated above.

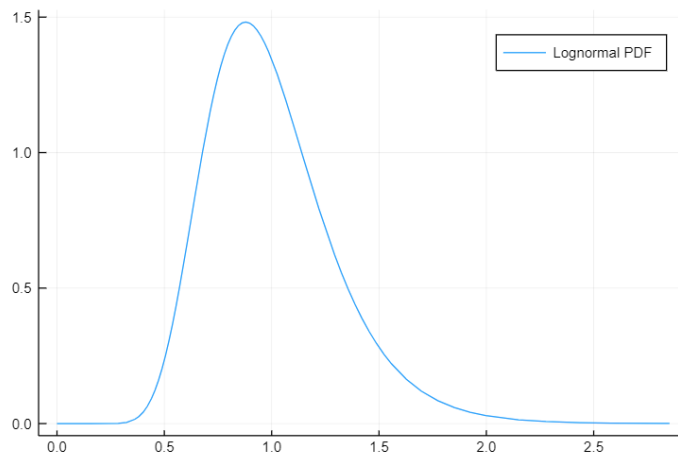


Figure 5-1 lognormal distribution

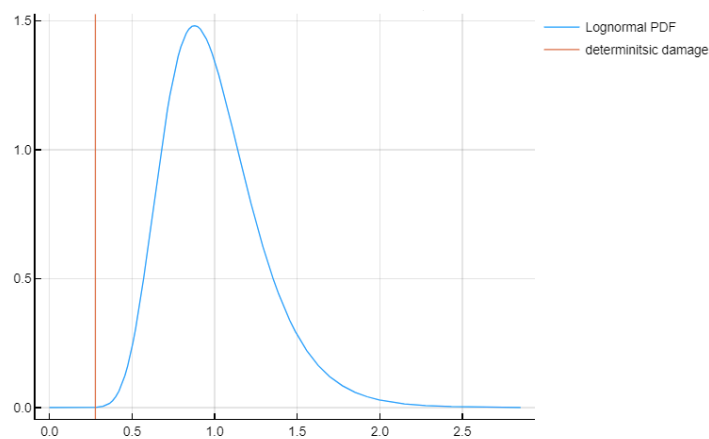


Figure 5-2 integrating lognormal with deterministic damage

The integration result is simply the area from $-\infty$ to the deterministic damage $[-\infty, 0.274]$. This area represents the probability of failure of the OC4 structure due to this damage. In this case, the probability of failure is equal to $9.9623 * 10^{-6}$.

5.4 Probability of Failure and Reliability

The total damage value is known from the damage distribution, therefore, the failure probability estimation is simply integrating the log-normal pdf with the deterministic total damage value.

As explained in the previous chapter, the parameters estimated for the log-normal are

$$\mu = -0.0431 \text{ and } \sigma = 0.2935$$

$$P_f = P(X \leq 0.27382) = \int_{-\infty}^{0.27382} f_X(y) dy$$

Where f_X is the pdf function, and y is the deterministic value.

$$P_f = 1 \times 10^{-5}$$

The reliability is then:

$$Reliability = 1 - P_f = 0.99999$$

5.5 Gaussian Process

The Gaussian Process, as implemented in Julia, is a function dependent on three different parameters. As explained in the previous chapter that the kernel is the most critical parameter of the three of them. The kernel is controlled by the length scale and the standard deviation.

For an accurate result, the length scale should be changed depending on a specific criterion. For the current case a length scale between 0.1 and 1.0 is used with an increment (0.1, 0.2, 0.3, ..., 1.0) value of 0.1.

One factor included in this Gaussian Process is the noise of the distribution. This noise prevents a zero variance at the chosen point, as shown in Figure 5-3, which affects the integration of the data points with the mean curve. Removing the noise from the distribution helps reshape the distribution and better fits with increasing the number of data points, as shown in Figure 5-4. However,

removing the noise from the Gaussian Process has the disadvantage of having a limited number of data points.

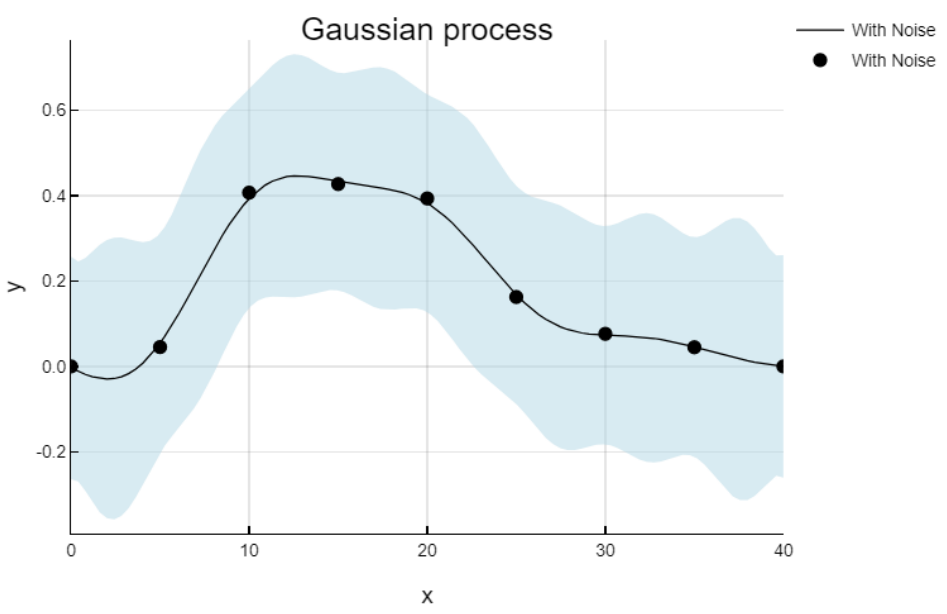


Figure 5-4 Gaussian Distribution with noise included

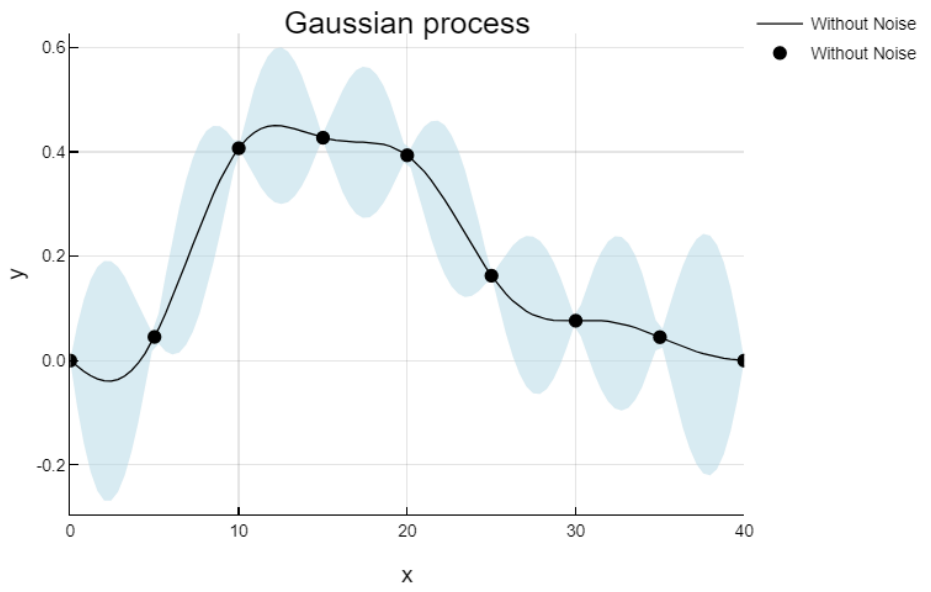


Figure 5-3 Gaussian Distribution without noise

5.5.1 The strategy of choosing observations

Knowing that in practice, the damage distribution is unknown and given only the probability density function with the wind speed, and the observations should be used depending on a particular strategy to define the damage curve accurately.

The strategy used in this thesis is to choose the points where the highest probabilities of the damage exist, starting with 5 points to check how the damage curve would look. The first plot was shown in Figure 5-5 below.

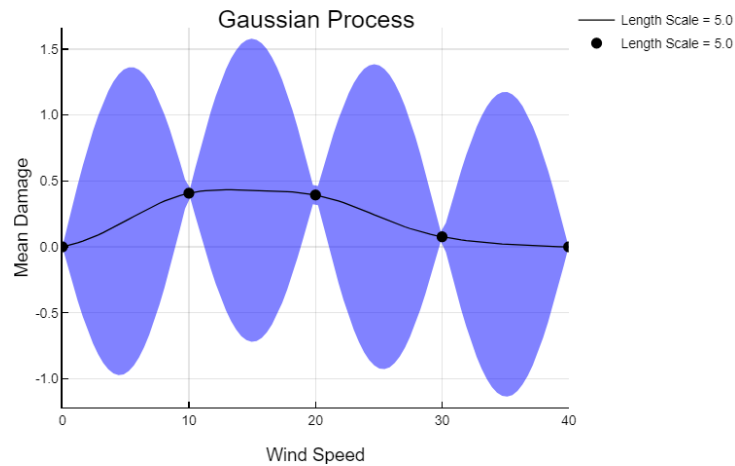


Figure 5-5 Damage Curve starting with 5 points

The uncertainty between every two points is as high as almost 1.5. The next step is to add a point where the highest uncertainty is at 5.005m/s. After adding this point, the distribution changes as follows

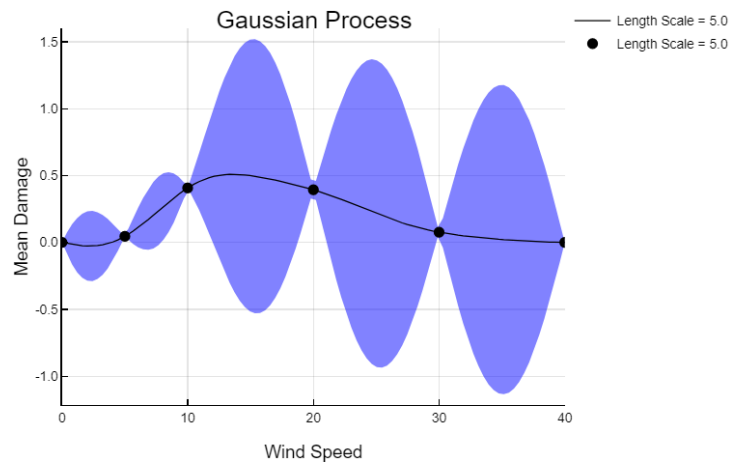


Figure 5-6 Damage Curve after adding a point

That shows that adding a point and replotting the distribution gives a hint on where to choose the next point. As mentioned previously in sub-chapter 3.8, the covariance matrix is always positive definite, and an issue appears when adding points using the same strategy at the highest uncertainty location with having a constant length scale of 1.0 results in allowing only 124 points to the graph. The reason behind the limited number of points is that for more than 124 points, the covariance matrix becomes negative definite, which is not allowable when implementing the Gaussian process. Using 65 observations to the distribution is shown in Figure 5-7

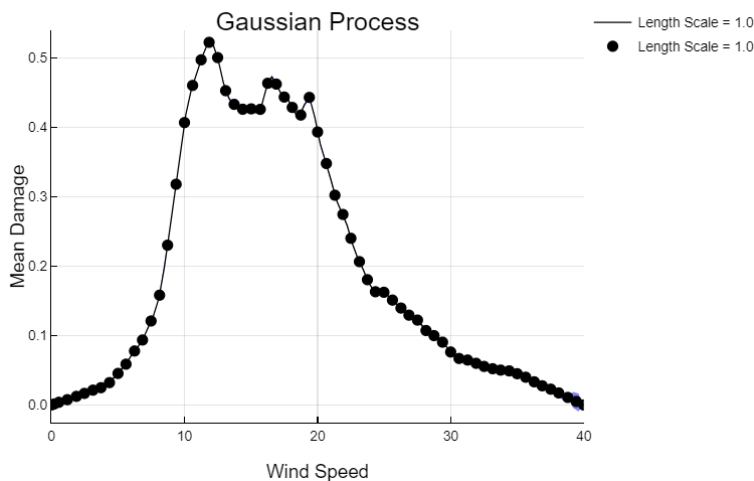


Figure 5-7 Damage Curve with 65 observations and length scale of 1.0

As discussed before, the more points being added to the distribution, the more accurate it becomes. Increasing the number of observations is done by decreasing the length scale. Figure 5-8 shows how the length scale changes the number of observations with having 1000 points as a maximum number of points.

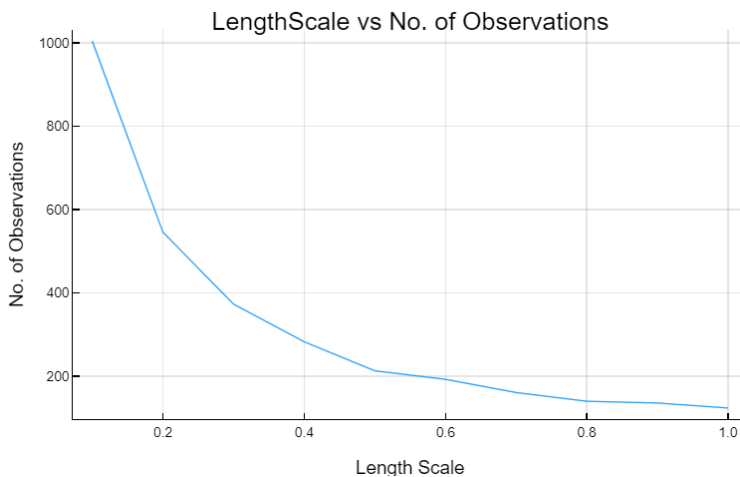


Figure 5-8 No. of observations vs length scale

As the graph above shows, the highest number of added points with the lowest length scale is around 200 points. The purpose of choosing these points is to have an accurate reliability value[46].

If the standard deviation is computed as a function of the length scale for a fixed number of 65 observations, we can notice the change in the standard deviation as shown in Figure 5-9 below

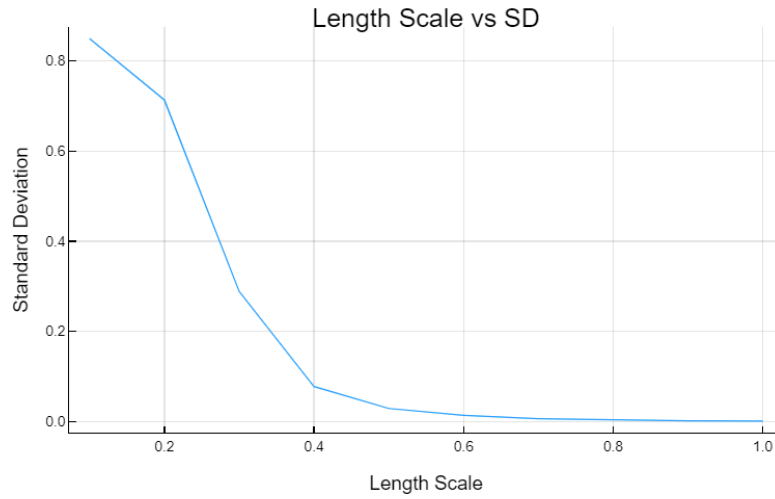


Figure 5-9 The length scale vs the standard deviation with having a constant number of points

Accordingly, the effect on the probability of failure can be seen as shown in Figure 5-10 below

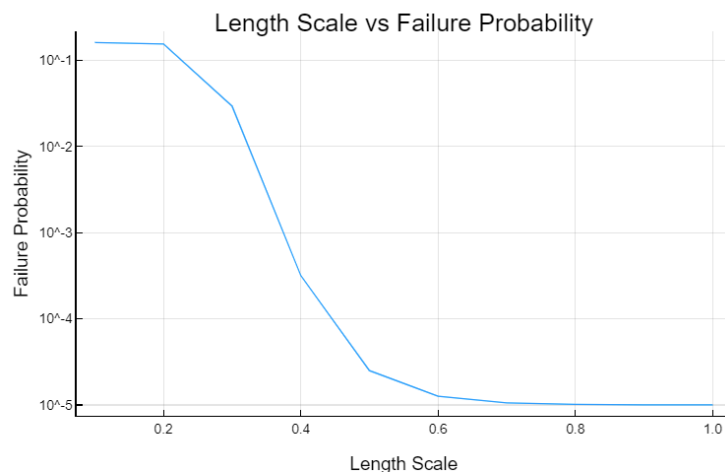


Figure 5-10 the relation between the length scale and the failure probability with having 65 data points

Using the available probability densities of the wind, the points that possess the highest probabilities are chosen to be inspected, as explained before. By adding the points, the probability of failure can be calculated by obtaining the mean and standard deviation of the gaussian process. Estimating the mean value of the Gaussian Process requires combining the damage curve with the probability densities. The integration of the resultant vector with the wind speeds gives the mean value needed.

$$\text{Gaussian Mean} = 0.274$$

Obtaining the standard deviation requires, first, calculating the total variance. The total damage D can be estimated as the sum of mean predicted damages d_i of each bin multiplied by the probability of occurrence p_i of the same bin.

$$D = \sum_{i=1}^N p_i d_i(x_i)$$

The expected total damage $E(D)$ can be calculated based on the mean damage estimates \hat{d}_i and their corresponding probability p_i similarly:

$$E(D) = E\left(\sum_{i=1}^N p_i d_i(x_i)\right) = \sum_{i=1}^N p_i E(d_i(x_i)) = \sum_{i=1}^N p_i \hat{d}_i(x_i)$$

Assuming that each location is independent of the other, which leads to an omitting of the covariances since these are zero for independent random variables. Since the covariances in the covariance matrix in the Gaussian process are all non-zero, this assumption cannot be applied anymore. The covariances must be included in the calculation of the variance.

Knowing that:

$$\text{Var}(X + Y) = \text{Var}X + \text{Var}Y + 2\text{Cov}(X, Y)$$

If N random variables X_i , with $i = 1 \dots N$, are considered, the variance of the sum of all random variables can be summarized as follows:

$$\text{Var}\left(\sum_{i=1}^N X_i\right) = \sum_{i=1}^N \sum_{j=1}^N \text{Cov}(X_i, X_j) = \sum_{i=1}^N \text{Var}(X_i) + 2 \sum_{1 \leq i < j \leq N} \text{Cov}(X_i, X_j)$$

This leads to the variance of the total damage:

$$\text{Var}(D) = \text{Var}\left(\sum_{i=1}^N p_i d_i(x_i)\right) = \sum_{i=1}^N \sum_{j=1}^N \text{Cov}(p_i d_i(x_i), p_j d_j(x_j))$$

Knowing that:

$$\text{Cov}(X, Y) = E(XY) - E(X)E(Y)$$

$$E(aX) = aE(X)$$

$$\begin{aligned} \text{Cov}(aX, bY) &= E(aXbY) - E(aX)E(bY) = abE(XY) - abE(X)E(Y) \\ &= ab(E(XY) - E(X)E(Y)) = ab\text{Cov}(X, Y) \end{aligned}$$

This leads to:

$$\text{Var}(D) = \sum_{i=1}^N \sum_{j=1}^N p_i p_j \text{Cov}(d_i(x_i), d_j(x_j)) = \sum_{i=1}^N p_i \sum_{j=1}^N \underbrace{p_j \text{Cov}(d_i(x_i), d_j(x_j))}_{\text{Kernel function}}$$

Looking at the covariance matrix (e.g. for $n = 3$), it can be seen that the above equation is the sum of all covariance elements (multiplied with p_i and p_j respectively).

$$\Sigma = \begin{bmatrix} \text{Var } X_1 & \text{Cov}(X_1, X_2) & \text{Cov}(X_1, X_3) \\ \text{Cov}(X_2, X_1) & \text{Var } X_2 & \text{Cov}(X_2, X_3) \\ \text{Cov}(X_3, X_1) & \text{Cov}(X_3, X_2) & \text{Var } X_3 \end{bmatrix}$$

The total variance is then:

$$\text{Var}(D) = 1.44 * 10^{-6}$$

The standard deviation is calculated as the square root of the variance

$$\text{Gaussian SD} = \sqrt{\text{Var}(D)} = 0.0012$$

The probability of failure is calculated by integrating CDF of the log-normal and PDF of the normal distribution of the gaussian mean and standard deviation.

$$\text{Failure Probability } (P_f) = 1.0 * 10^{-5}$$

The reliability is then calculated as:

$$Reliability = 1 - P_f = 0.9999899$$

Adjusting the parameters of the Gaussian Process is of great importance. These parameters are shaping the gaussian distribution and indicating if the training points are in the correct location or not.

The results are obtained with having a length scale of 1.0, 65 observations, and a noise value of 0. It is required to have reliability within the standard limit, as explained earlier. The probability of failure starts to converge, and the change becomes very small, beginning with 35 points, and adding one more point changes the reliability by less than 0.0002%.

The number of observations is limited for every chosen length scale. However, adding the noise to the process allows an infinite number of data points. The question is, how many data points are needed to have an accurate and reliable solution? The answer to this can be explained by plotting the Gaussian Process with a different number of data points.

Using noise of 0.05 as a constant and choosing 100 data points, we get

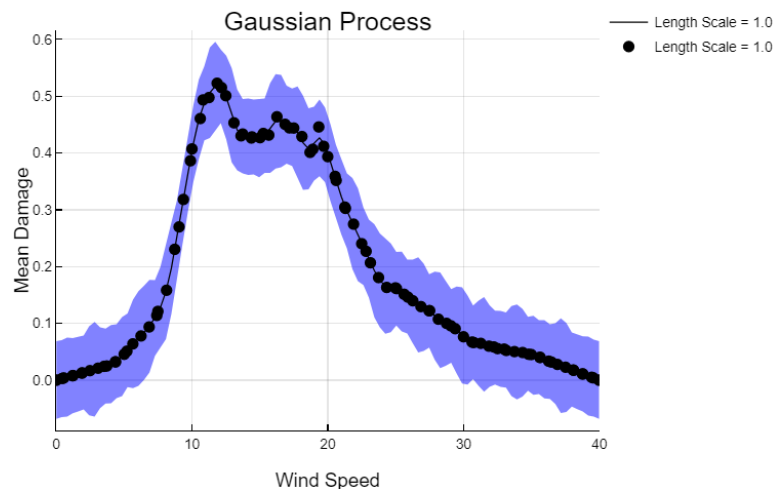


Figure 5-11 Gaussian Process with 0.05 noise and 100 data points

$$Mean = 0.2738$$

$$SD = 0.073$$

$$P_f = 0.00026$$

$$Reliability = 0.99974$$

Using 200 data points, we get

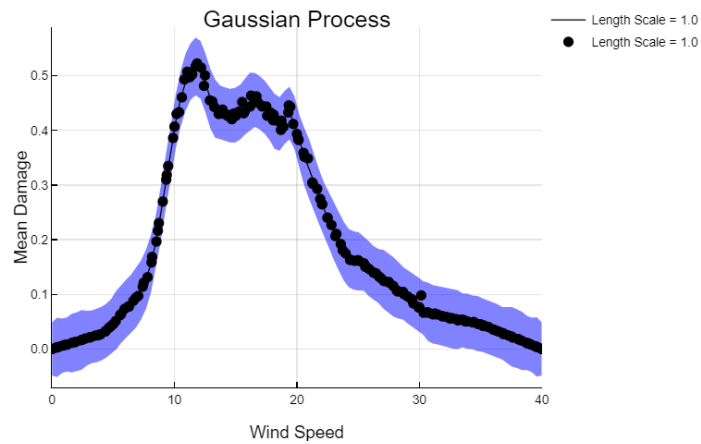


Figure 5-12 Gaussian Process with 0.05 noise and 200 data points

$$\text{Mean} = 0.2739$$

$$SD = 0.05$$

$$P_f = 7.95 * 10^{-5}$$

$$\text{Reliability} = 0.9999205$$

However, increasing the number of data points will reduce the failure probability and increase the reliability until it converges to the same value obtained without the noise at about 500 observations. Although the number of data points affects the standard deviation and the reliability, an alternative solution is having constant data points and changing the noise. Reducing the noise and increasing

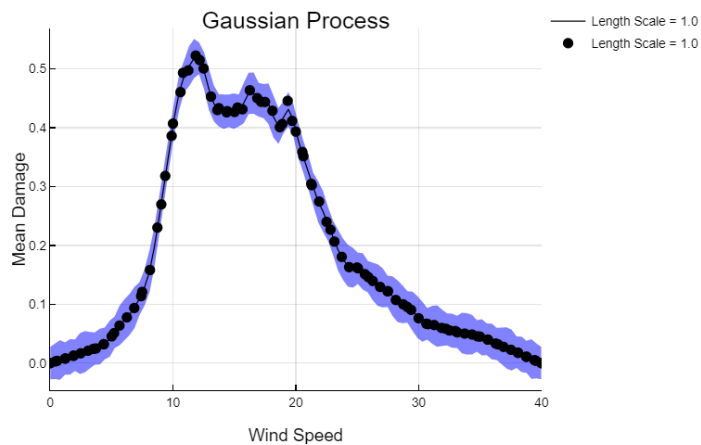


Figure 5-13 Gaussian Process with 0.02 noise and 100 data points

it changes the uncertainty of the distribution. If we have 100 data points and reduce the noise to 0.02, for instance, we get

$$\text{Mean} = 0.2739$$

$$\text{SD} = 0.0292$$

$$P_f = 2.4 * 10^{-5}$$

$$\text{Reliability} = 0.999976$$

This also shows that the change of noise influences the reliability as reducing the noise increases the reliability, and decreasing it increases the reliability value.

If we have a constant number of data points, the standard deviation changes accordingly, as shown in Figure 5-14 below

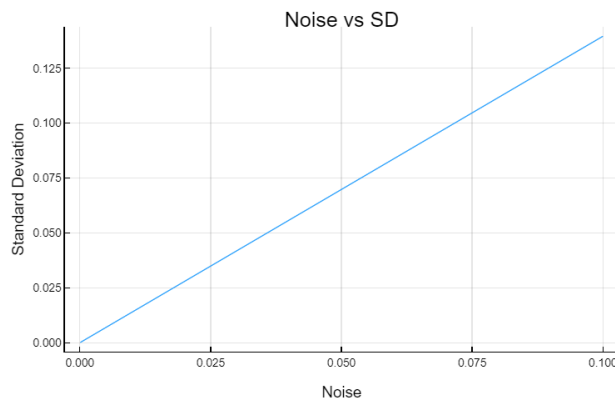


Figure 5-14 Relation between the noise and standard deviation with having 100 data points

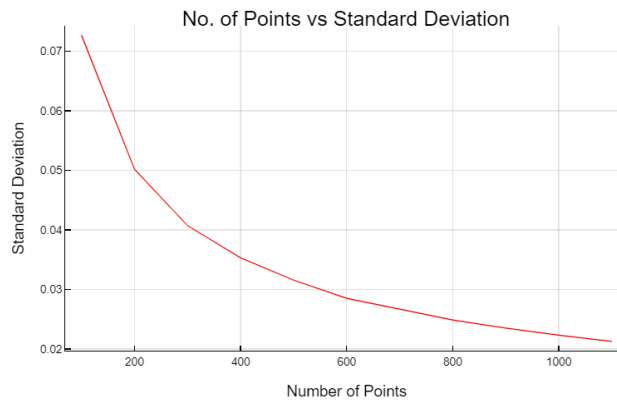


Figure 5-15 Relation between the standard deviation and the no. of points with having a constant noise of 0.05

Accordingly, if we have a fixed noise, for instance, of 0.05 and we change the number of observations, we can notice the change of the standard deviation as shown in Figure 5-15 above.

Using the same comparison with the reliability instead of the standard deviation, for constant noise, we can see the decrement of the probability of failure as shown in Figure 5-17 below

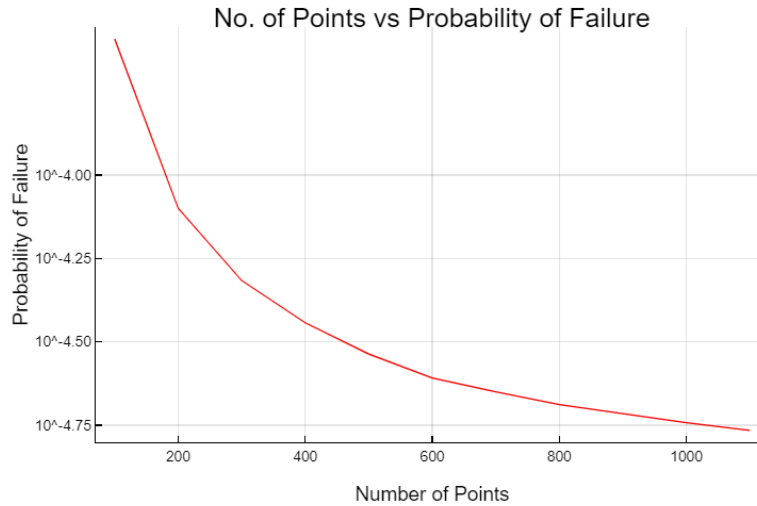


Figure 5-17 the relation between no. of points and the probability of failure with having constant noise of 0.05

Similarly, we can see the change of the reliability with changing the noise while having a constant number of data points, as shown in Figure 5-16 below

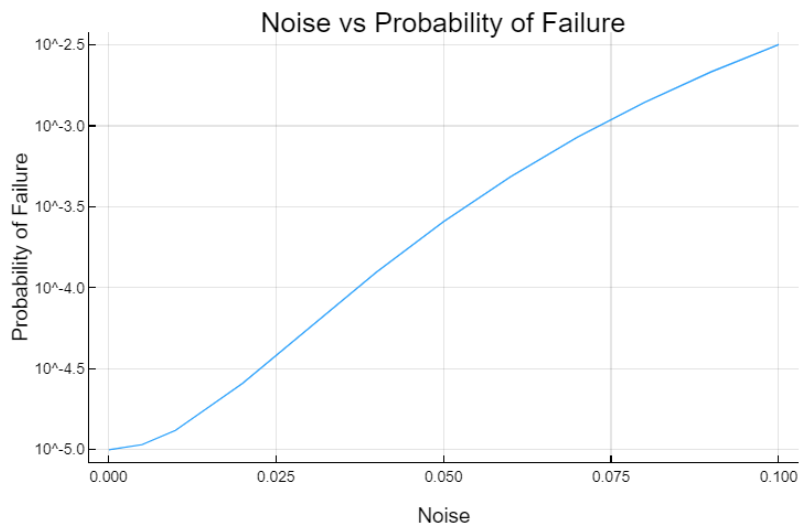


Figure 5-16 the relation between the noise and reliability with having 100 data points

The above curves show how the number of observations differs by changing the hyperparameters of the Gaussian Process. With the right choice of hyperparameters, one can reach the desired results with the minimum number of observations. As explained earlier, if the noise is removed, an accurate value of failure probability can be achieved using 35 points in the Gaussian distribution. The exact value can be reached by adding slight noise and more than 500 observations. As the goal is to achieve the desired reliability with the minimum number of observations, it would be more efficient and economical to use the method with fewer points.

Chapter 6: Discussion

Although the Gaussian Process has some challenges, the results obtained using this approach, however, show that structural reliability can be obtained using a significantly small number of data points instead of the hundreds and thousands of load-response simulations used in traditional numerical methods. The challenge faced is the control of the hyperparameters of the Gaussian Process together at the same time. Each of these parameters has an effect on the distribution of the observations chosen.

6.1 Effect of Length Scale

The length scale showed how it could control the distribution from possessing high error or almost zero error. Changing the length scale changes the number of observations and, consequently, the shape of the distribution.

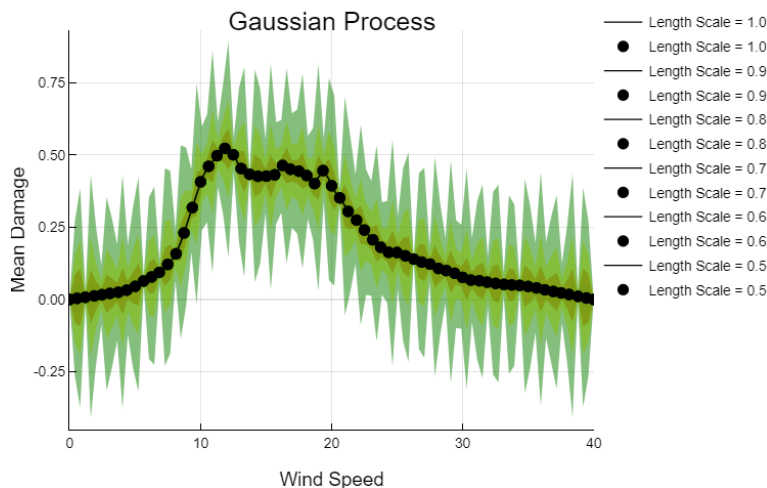


Figure 6-1 Gaussian distribution with different length scales

As explained in the previous chapter, the lower the length scale is, the more points can be added. Having a small length scale with a low number of observations can lead to having a high failure probability. It would be more accurate to have a constant length scale, 0.5, for instance, and keep adding points until the results converge with the desired failure probability.

6.2 Effect of Noise

Although the noise, in a way, does not allow perfect fitting of the mean curve of the gaussian distribution with the data points, it will enable adding as many data points as needed to estimate the structure's accurate probability of failure and reliability. As shown in the results, the noise

effect cannot be ignored if more data points are needed to be added. The larger the noise, the more error exists in the distribution.

For a small error, a minimal value of noise is allowed to exist in the Gaussian Process. Increasing the noise showed an increase in the error of the distribution. Adding more points contributed to having a more accurate result, but the more points added to the process, the more reliable the system becomes. The convergence of the failure probability happens after 200 to 300 data points. That means that it is neither necessary nor efficient to add more points to the process with so little change happening to the failure probability. The challenge faced by controlling noise is changing the noise with the number of points as both of them contribute to reducing the error. Choosing a suitable noise value is the main challenge in this case. A proper noise value selected in this case is a noise of 0.05. A fixed 0.05 noise made the convergence of the failure probability possible at 500 points, which means adding more than 500 points would not be efficient in evaluating the structural reliability.

6.3 Convergence

A good strategy implemented using the Gaussian Process is to keep the noise = 0 and start with a small number of observations, five observations, and keep adding points until the probability of failure converges. By that, it is meant that the more points are added, the less the change of the failure probability.

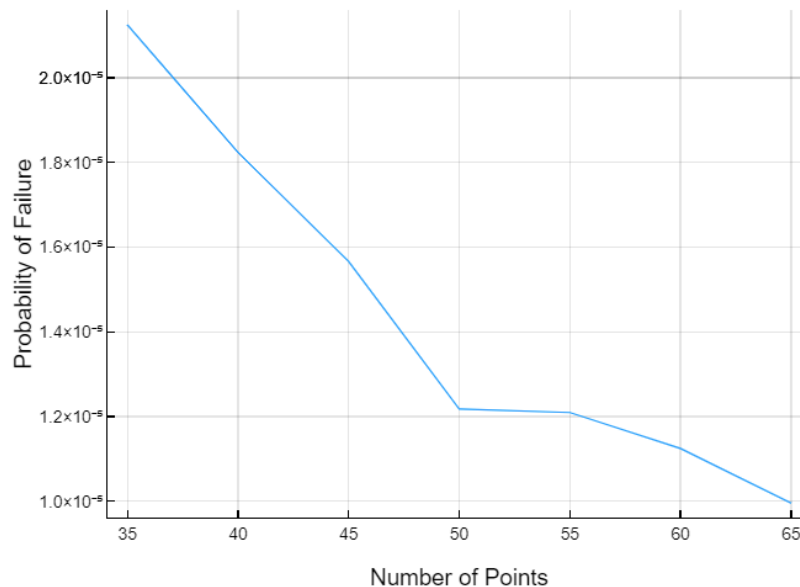


Figure 6-2 convergence of the failure probability

As shown in Figure 6-2 above, the change in the failure probability is as low as $2 * 10^{-6}$ every five added points.

Eventually, comparing the Gaussian Process to the other deterministic methods shows that the Gaussian Process achieves the desired results with significantly lower observations.

Table 6-1 Comparison between the different methods of obtaining the probability of failure

	Bins Method	Monte Carlo Integration	Numerical Integration	Gaussian Process
Number of Points	1,000	1,000,000	10,000	65
Probability of Failure	$1 * 10^{-5}$			
Mean Damage	0.274			

Chapter 7: Conclusion, Recommendation, and Further Work

The Gaussian Process is showing promising results in obtaining accurate fatigue reliability. With fewer load-response simulations, it is possible to achieve the desired failure probability with a high level of accuracy. Controlling the hyperparameters is the primary key to reaching the objective required.

Comparing the Gaussian Process to other methods, such as Monte Carlo Integration, Bins method, and Numerical Integration shows significant accuracy in the calculations with a significantly smaller number of data points, which makes this approach efficient in terms of time consumption and cost.

The Gaussian Process approach is performing, compared to the currently used methods in the industry, relatively well. Challenges implementing the Gaussian Process, controlling the hyperparameters, can be handled using efficient strategies.

7.1 Recommendations

7.1.1 Points Selection

A practical strategy is to start with defining the selected points of the Gaussian distribution. An advantage of using the Gaussian Process is that it shows the variance in the distribution plot. The highest variance value is the position of interest to add one more point to the distribution. Replotting the distribution with the added point would show the following location to add more points. This strategy helps to reduce the error significantly rather than choosing random points at random locations of the distribution.

7.1.2 Convergence

Adding points lead to having more accurate results. A strategy to know where to stop adding points or indicate having enough points would be the convergence of the probability of failure. If the change in the likelihood of failure that occurs by adding points is too low, the process of adding more points can be stopped.

A low difference is that the change is happening to the 4th or the 5th digit only. The convergence value used in this thesis was 0.0001. Consequently, a change below this value indicates that adding more points to the process is unnecessary.

7.2 Further Work

- Using a different type of hyperparameters optimization for more accuracy and efficiency.
- Using a different type of kernel function and how it would influence the whole Gaussian process and the outputs.
- The Gaussian Process is implemented on one dimension, wind loading, in this thesis. It would be exciting and beneficial to add another dimension, wave loading, for instance, to the process and test its accuracy under different conditions.

References

- [1] C. Zhu and Y. Li, *Reliability Analysis of Wind Turbines*. IntechOpen, 2018. doi: 10.5772/intechopen.74859.
- [2] N. Jensen and C. WWF-Norway, “challenge: We need to contain global warming to hinder catastrophic consequences for people and nature. Luckily we already know what needs to be done: The global energy production needs to be shifted from fossil to renewable energy. How we make this shift, will have everything to say for its success.,” p. 25.
- [3] F. Fu, “Chapter Eight - Design of Offshore Structures,” in *Design and Analysis of Tall and Complex Structures*, F. Fu, Ed. Butterworth-Heinemann, 2018, pp. 251–293. doi: 10.1016/B978-0-08-101018-1.00008-3.
- [4] J. G. Speight, “Chapter 3 - Offshore Platforms,” in *Subsea and Deepwater Oil and Gas Science and Technology*, J. G. Speight, Ed. Boston: Gulf Professional Publishing, 2015, pp. 71–106. doi: 10.1016/B978-1-85617-558-6.00003-9.
- [5] C. Golightly, “Monopile and Tripod/Jacket Foundations for Offshore Wind Foundations April 2014”, Accessed: May 01, 2021. [Online]. Available: https://www.academia.edu/6952015/Monopile_and_Tripod_Jacket_Foundations_for_Offshore_Wind_Foundations_April_2014
- [6] A. Taheri and G. Emamverdizadeh beyg, “Effect of Pile Scouring on the Structural Behavior of a Fixed Jacket Platform with Consideration of Non-linear Pile Seabed Interaction,” *J. Rehabil. Civ. Eng.*, no. Online First, Sep. 2017, doi: 10.22075/jrce.2017.12150.1206.
- [7] L. Drummond, M. Mulcahy, and S. Culloty, “The reproductive biology of the Manila clam, *Ruditapes philippinarum*, from the North-West of Ireland,” *Aquaculture*, vol. 254, no. 1, pp. 326–340, Apr. 2006, doi: 10.1016/j.aquaculture.2005.10.052.
- [8] A. Lapworth, “The diurnal variation of the marine wind in an offshore flow,” *Q. J. R. Meteorol. Soc.*, vol. 131, pp. 2367–2387, Dec. 2006, doi: 10.1256/qj.04.161.
- [9] Ö. Halici and H. Mutungi, “Assessment of simulation codes for offshore wind turbine foundations,” 2016.
- [10] P. S. Maran, “Meteorological tower wind shear characteristics, vertical wind speed profile, and surface roughness analysis near the coastline of Chennai,” p. 6, 2019.
- [11] E. Petersen, N. Mortensen, L. Landberg, and H. Frank, “Wind Power Meteorology,” Jan. 1997.

- [12] A. Abdalla, W. El-Osta, and E. Dekam, *The Influence Of The Atmospheric Stability Conditions On The Available Wind Energy For Three Libyan coastal Cities*. 2017.
- [13] M. L. Hossain, A. Abu-Siada, and S. M. Muyeen, “Methods for Advanced Wind Turbine Condition Monitoring and Early Diagnosis: A Literature Review,” *Energies*, vol. 11, no. 5, Art. no. 5, May 2018, doi: 10.3390/en11051309.
- [14] E. L. Petersen, *1999 European Wind Energy Conference: Wind Energy for the Next Millennium*. Routledge, 2014.
- [15] B. Hahn, M. Durstewitz, and K. Rohrig, “Reliability of wind turbines: Experiences of 15 years with 1,500 WTs,” *Fraunhofer IWES*, Jan. 2006.
- [16] S. Faulstich, B. Hahn, and P. J. Tavner, “Wind turbine downtime and its importance for offshore deployment,” *Wind Energy*, vol. 14, Apr. 2011, doi: 10.1002/we.421.
- [17] J. Lindsay, D. Briand, R. R. Hill, J. A. Stinebaugh, and A. S. Benjamin, “Wind turbine reliability : a database and analysis approach.,” SAND2008-0983, 1028916, Feb. 2008. doi: 10.2172/1028916.
- [18] B. H. Chudnovsky, *Transmission, Distribution, and Renewable Energy Generation Power Equipment: Aging and Life Extension Techniques, Second Edition*. CRC Press, 2017.
- [19] D. S. Saini, D. Karmakar, and S. ray chaudhuri, “A Review of Stress Concentration Factors in Tubular and Non-Tubular Joints for Design of Offshore Installations,” *J. Ocean Eng. Sci.*, vol. 1, Aug. 2016, doi: 10.1016/j.joes.2016.06.006.
- [20] B. Yong and J. Wei-Liang, *Marine Structural Design*. Elsevier, 2016. doi: 10.1016/C2013-0-13664-1.
- [21] S. W. Smith, *The scientist and engineer’s guide to digital signal processing*. San Diego, Calif.: California Technical Pub., 1999.
- [22] J. V. Kemble, “PH changes on the surface of burns,” *Br. J. Plast. Surg.*, vol. 28, no. 3, pp. 181–184, Jul. 1976, doi: 10.1016/0007-1226(75)90126-5.
- [23] H. Holzer, “Chemistry and biology of macromolecular inhibitors from yeast acting on proteinases A and B, and carboxypeptidase Y,” *Adv. Enzyme Regul.*, vol. 13, pp. 125–134, 1974, doi: 10.1016/0065-2571(75)90011-4.
- [24] H. R. Maier, B. J. Lence, B. A. Tolson, and R. O. Foschi, “First-order reliability method for estimating reliability, vulnerability, and resilience,” *Water Resour. Res.*, vol. 37, no. 3, pp. 779–790, Mar. 2001, doi: 10.1029/2000WR900329.

- [25] A. Halder and S. Mahadevan, “Probability, Reliability, and Statistical Methods in Engineering Design | Wiley,” *Wiley.com*. <https://www.wiley.com/en-us/Probability%2C+Reliability%2C+and+Statistical+Methods+in+Engineering+Design-p-9780471331193> (accessed Jun. 14, 2021).
- [26] S. Maskey and V. Guinot, “Improved first-order second moment method for uncertainty estimation in flood forecasting,” *Hydrol. Sci. Journal*, vol. 48, pp. 183–196, Apr. 2003, doi: 10.1623/hysj.48.2.183.44692.
- [27] R. E. Melchers and A. T. Beck, *Structural reliability analysis and prediction*, Third edition. Hoboken, NJ: Wiley, 2018.
- [28] “DNVGL-OS-C101.pdf.” Accessed: Apr. 30, 2021. [Online]. Available: <https://rules.dnvgl.com/docs/pdf/dnvgl/os/2015-07/DNVGL-OS-C101.pdf>
- [29] B. Liu and L. Xie, “An Improved Structural Reliability Analysis Method Based on Local Approximation and Parallelization,” *Mathematics*, vol. 8, no. 2, p. 209, Feb. 2020, doi: 10.3390/math8020209.
- [30] H. Zhang, H. Dai, M. Beer, and W. Wang, “Structural reliability analysis on the basis of small samples: An interval quasi-Monte Carlo method,” *Mech. Syst. Signal Process.*, vol. 37, pp. 137–151, May 2013, doi: 10.1016/j.ymsp.2012.03.001.
- [31] H. Ray, “Sturge’s Rule; A Method for Selecting the Number of Bins in a Histogram,” *Accendo Reliability*, Aug. 11, 2020. <https://accendoreliability.com/sturges-rule-method-selecting-number-bins-histogram/> (accessed Jun. 04, 2021).
- [32] V. Cumer, “The basics of Monte Carlo integration,” *Medium*, Nov. 06, 2020. <https://towardsdatascience.com/the-basics-of-monte-carlo-integration-5fe16b40482d> (accessed Jun. 05, 2021).
- [33] M Muskulus and S Schafhirt, “Reliability-based design of wind turbine support structures,” 2015, doi: 10.13140/RG.2.1.5125.5766.
- [34] H. Li, Y. He, and X. Nie, “Structural reliability calculation method based on the dual neural network and direct integration method,” *Neural Comput. Appl.*, vol. 29, no. 7, pp. 425–433, Apr. 2018, doi: 10.1007/s00521-016-2554-7.
- [35] A. Francisco, J. A. Duran, C. Vilela, and T. Simões, *Comparison of Numerical Integration and Monte Carlo Simulation Methods for Structural Reliability based on the Failure Assessment Diagram*. 2015. doi: 10.20906/CPS/CILAMCE2015-0416.

- [36] J. Görtler, R. Kehlbeck, and O. Deussen, “A Visual Exploration of Gaussian Processes,” *Distill*, vol. 4, no. 4, p. e17, Apr. 2019, doi: 10.23915/distill.00017.
- [37] S. Yuge, “Gaussian Processes, not quite for dummies,” *The Gradient*, Nov. 13, 2019. <https://thegradient.pub/gaussian-process-not-quite-for-dummies/> (accessed Jun. 10, 2021).
- [38] D. Baccanari, A. Phillips, S. Smith, D. Sinski, and J. Burchall, “Purification and properties of *Escherichia coli* dihydrofolate reductase,” *Biochemistry*, vol. 14, no. 24, pp. 5267–5273, Dec. 2015, doi: 10.1021/bi00695a006.
- [39] J. Butler, G. G. Jayson, and A. J. Swallow, “The reaction between the superoxide anion radical and cytochrome *c*,” *Biochim. Biophys. Acta*, vol. 408, no. 3, pp. 215–222, Dec. 2016, doi: 10.1016/0005-2728(75)90124-3.
- [40] A. Schmoldt, H. F. Bente, and G. Haberland, “Digitoxin metabolism by rat liver microsomes,” *Biochem. Pharmacol.*, vol. 24, no. 17, pp. 1639–1641, Sep. 2017.
- [41] L. Kang, R.-S. Chen, N. Xiong, Y.-C. Chen, Y.-X. Hu, and C.-M. Chen, “Selecting Hyper-Parameters of Gaussian Process Regression Based on Non-Inertial Particle Swarm Optimization in Internet of Things,” *IEEE Access*, vol. 7, pp. 59504–59513, 2019, doi: 10.1109/ACCESS.2019.2913757.
- [42] S. Bartels and P. Hennig, “Conjugate Gradients for Kernel Machines,” p. 42.
- [43] G. Su, J. Jiang, B. Yu, and Y. Xiao, “A Gaussian process-based response surface method for structural reliability analysis,” *Struct. Eng. Mech.*, vol. 56, pp. 549–567, Nov. 2015, doi: 10.12989/sem.2015.56.4.549.
- [44] C. E. Rasmussen and C. K. I. Williams, *Gaussian processes for machine learning*. Cambridge, Mass: MIT Press, 2006.
- [45] Z. Daniel and M. Michael, “Simplified fatigue load assessment in offshore wind turbine structural analysis”, doi: 10.1002/we.1831.
- [46] G. Sigurdsson, E. Cramer, I. Lotsberg, B. Berge, and Ø. Hagen, “Guideline for Offshore Structural Reliability,” *Tech. Rep.*, no. 95, p. 80.

Appendix

Julia Script

This script is written using Julia version 1.5.3.

```
using NumericalIntegration
using QuadGK
using Distributions
import Random: randn, MersenneTwister
# Probability density function for the wind
"""
    weibull(beta,eta,gamma,x)
Returns the Weibull distribution for `x`.
`beta` ... Shape parameter (or slope)
`eta` ... Scale parameter
`gamma` ... Location parameter; frequently not used
"""
function weibull( beta::AbstractFloat,
                  eta::AbstractFloat,
                  gamma::AbstractFloat,
                  x::Array{<:AbstractFloat,1})
    return beta/eta*((x.-gamma)/eta).^(beta-1).*exp(-((x.-gamma)/eta).^beta)
end
# version for x as Float64
function weibull( beta::AbstractFloat,
                  eta::AbstractFloat,
                  gamma::AbstractFloat,
                  x::AbstractFloat)
    return weibull(beta, eta, gamma, [x])[1]
end
# Parameter for the Upwind Deepwater-Site
beta = 2.04
eta = 11.75
gamma = 0.0
# Define wind distribution function as function depending only on wind speed v
```

```

upwindDistr(v) = weibull(beta,eta,gamma,v)

"""
    linearInterpolation(xarray, yarray, interpolateX)
Linear interpolation between two values.
# Example
```julia-repl
julia> linearInterpolation([1, 2], [0, 4], 1.5)
2.0
```
"""
function linearInterpolation(xarray::Array{Float64,1},yarray::Array{Float64,1},
                            interpolateX::Float64)
    minX, maxX = minimum(xarray), maximum(xarray)
    # Check argument in bounds
    minX <= interpolateX <= maxX || error("Input value out of bounds, no interpola
tion possible!")
    interpolateX == maxX && return yarray[end]
    # Location in array which is below interpolation value
    loc1 = findall(x -> x<=interpolateX, xarray)[end]
    # Linear interpolation
    x1, x2 = xarray[loc1], xarray[loc1+1]
    y1, y2 = yarray[loc1], yarray[loc1+1]
    return interpolateY = (interpolateX-x1)/(x2-x1)*(y2-y1)+y1
end
# Version for Array input
function linearInterpolation(xarray::Array{Float64,1},yarray::Array{Float64,1},
                            interpolateX::Array{Float64,1})
    interpolateY = Float64[]
    for i in interpolateX
        push!(interpolateY, linearInterpolation(xarray,yarray,i))
    end
    return interpolateY
end
# Int version

```

```

function linearInterpolation(xarray::Array{Float64,1},yarray::Array{Float64,1},
                             interpolateX::Int64)
    return linearInterpolation(xarray, yarray, Float64(interpolateX))
end
"""
    createDamageData()
Generates the artificial damage results for wind speeds between 0 and 40 m/s.
- returns 2 1D arrays: windVelocity and damage
"""
function createDamageData(;deltaV = 0.05, noiseRatio = 0.025)
    # Raw data from Zwick, Muskulus
    # Simplified fatigue load assessment in offshore wind turbine structural analysis
    # Figure 3 - level 5
    rawdata = [
    # Linear assumption to zero velocity
    0.0      0.0;
    # Data from paper
    3.99304 0.00761;
    5.00209 0.01269;
    6.00418 0.02081;
    7.00626 0.02690;
    7.99443 0.04061;
    8.99652 0.07310;
    9.99861 0.11472;
    11.0007 0.14112;
    12.0027 0.14365;
    13.0048 0.12995;
    14.0069 0.12132;
    # artificial peak #1
    14.2000 0.14021;
    14.3000 0.11903;
    # end
    14.9951 0.12030;
    15.9972 0.12335;

```

```

16.9993 0.12843;
19.0034 0.11168;
# artificial peak #2
19.2000 0.13579;
19.3000 0.12403;
# end
20.9937 0.08985;
24.0069 0.04924;
# made up data for higher wind speeds
29.0    0.02690;
30.0000 0.02081;
# artificial peak #3
30.2000 0.03021;
30.3000 0.01903;
# end
35.0000 0.01269;
40.0000 0.00000]

rawdata[:,2] = rawdata[:,2]*3.554648550953938

# Add noise
# Random number generator with constant seed
rng = MersenneTwister(123456);

# Wind speed array
# from 0 m/s to 40 m/s, every 0.05 m/s
windVelocity = collect(0:deltaV:40)
l=length(windVelocity)

damages = Float64[]
for i in windVelocity
    velocity = linearInterpolation(rawdata[:,1],rawdata[:,2],i)
    noise = noiseRatio*velocity*randn(rng)
    push!(damages,velocity+noise)
end

```

```

    return windVelocity, damages
end

# example plot of wind distribution and damage data
import Plots
# Generate the wind velocity and damage arrays
v, d =createDamageData();
# Generate the Weibull PDF for the given wind velocity array
p = upwindDistr(v);
p1 = Plots.plot(v,p, xlabel="wind speed [m/s]", label="Weibull distribution", lw=
2, linecolor = :black)
p2 = Plots.plot(v,d, xlabel="wind speed [m/s]", label="Damage curve", lw=2)
Plots.plot(p1, p2, layout=(2,1))

# 2020-03-10: Additional linearInterpolation possibilities
# getting return value inbetween two values, x as Float64
linearInterpolation(v,d,3.12341234)
# getting return value inbetween two values, x as Int64
linearInterpolation(v,d,3)
# getting return value inbetween two values, x as Array of Floats
linearInterpolation(v,d,[3.12341234, 17.12334, 33.12])

#damage with bins
using Distributions
using QuadGK
function BinsDam(N)
    step = floor(Int, length(v)/N)      #defining the step between each point
    speed = v[1:step:end]
    speed2=Float64[]
    Pdf=[]          #empty array to push in the probabilities
    for i in 1:N
        spd = (speed[i]+speed[i+1])/2
        push!(speed2 , spd)
    end
end

```



```

        IntDmg = linearInterpolation(v,d, speed2)           #getting the damage for
every wind speed using linear interpolation
        for i in 1:N
            pdfspd = quadgk(upwindDistr, speed[i], speed[i+1])[1]   #calculating
the probabilities through the integration of the probability densities
            push!(Pdf,pdfspd)
        end
        Totaldamage=[]           #empty array to push in the total damage
        for j in 1:N
            totaldmg = IntDmg[j]*Pdf[j]
            push!(Totaldamage, totaldmg)
        end
        return Totaldamage
    end
sum(BinsDam(500))

#Monte Carlo Integration method

function MonteCarloInt(Rn)
    Randspeed = sort(rand(Uniform(0,40),Rn))           #generating random numbers
from 0 to 40 m/s
    RandomDmg = linearInterpolation(v,d, Randspeed)     #getting the damage u
sing the linear interpolation
    prob=[]           #empty array to push in the probabilities
    MtDmg=[]           #empty array to push in the damage
    for i in 1:Rn-1
        pdf=quadgk(upwindDistr, Randspeed[i],Randspeed[i+1])[1]
        push!(prob,pdf)
    end
    for j in 1:Rn-1
        montecarlo = RandomDmg[j]*prob[j]
        push!(MtDmg, montecarlo)
    end
    return(MtDmg)
end

```

```

sum(MonteCarloInt(1000000))

using StatsPlots
using Plots
plot(Normal(1, 0.3), label="pdf")
plot!(Normal(1, 0.3), func=cdf, label="cdf")

#the numerical integration method

function NumInteg(S)
    vel = [0:S:40;]
    interpolateddmg(vel) = linearInterpolation(v,d, vel)
    combinedcurve(vel)=interpolateddmg(vel)*upwindDistr(vel)           #combining the
damage with probability densities
    results=[]
    for i in 1:length(vel)-1
        int = quadgk(combinedcurve, vel[i], vel[i+1])[1]
        push!(results, int)
    end
    return results
end
sum(NumInteg(0.004))

using StatsBase
using StatsFuns
probs=[]
for i in 1:length(v)-1
    pdf = quadgk(upwindDistr, v[i], v[i+1])[1]
    push!(probs, pdf)
end
t= plot(Normal(1, 0.3))
t2=plot(v[1:end-1],cumsum(probs))
plotly()
Plots.PlotlyBackend()

```

```

miuD = -0.0431          #miu of the log-normal
sigmaD = 0.2935         #sigma of the log-normal

plot(LogNormal(miuD, sigmaD), func= cdf)
roll=LogNormal(miuD, sigmaD)
plot(roll , label="Lognormal PDF")
vline!([0.278], label="deterministic damage")
Pf = quadgk(x->pdf(roll,x), 0,sum(NumInteg(0.004)))[1]
reliability = 1-Pf

using GaussianProcesses
import LinearAlgebra: diag
R=Float64[0.0, 10.0, 20.0, 30.0, 40.0]          #array with the initially chosen points

#a function to generate the data of the gaussian process

function gendata(x)
    y= linearInterpolation(v,d,x)
    kernel=SE(log(1.0),log(1.0))          #the kernel function of the gaussian process
    ss
    Mean=MeanZero()
    LogNoise = log(0.05)
    gaussianprocess= GP(x, y, Mean, kernel, LogNoise)

    rangeval = range(0,stop=40,length=1000)          #dividing the wind speed into 1000 segments
    rangevalue = [0.0:0.04004004004004004:40.0;]
    meanval, CoVmatrix = predict_f(gaussianprocess,rangeval;full_cov=true);
    varval = abs.(diag(CoVmatrix))
    return meanval, varval, rangevalue, sum(CoVmatrix)
end

```

```

#function to locate the maximum variance value in the gaussian distribution

function Locatevar(wind,Var)
    return wind[findmax((Var)[1:end])[2]]
end

#function to add the point corresponding to the maximum variance to the initially
selected points (R)

function Addingpt(R, newlocation)
    G = push!(R,newlocation)
    return sort(G)
end

#a function collecting the previous three functions to generate the points automa
tically into "R" array
function DataPoints(s)
    R=sort(R)
    Mean,Var,wind,totVar=gendata(R)
    Maxvarpt=Locatevar(wind,Var)
    Addingpt(R,Maxvarpt)
    return R
end
DataPoints(R)

#Function to calculate the Gaussian Process reliability

function GaussianRel(z,v,d)
    y= linearInterpolation(v,d,z)           #linear interpolation to calcula
te the damage at the chosen wind speeds
    kernel=SE(log(1.0),log(1.0))           #Kernel function of the Gaussian
Process
    Mean=MeanZero()                         #mean function of the Gaussian P
rocess

```

```

LogNoise = log(0.0) #the noise of the Gaussian Process
ss set to zero
gaussianprocess= GP(z, y, Mean, kernel, LogNoise) #generating the Gaussian
Process data
rangeval = range(0,stop=40,length=1000) #rangeval divides the wi
nd speeds into a desired number of points
rangevalue = [0.0:0.04004004004004004:40.0;]
meanval, CovMtx = predict_f(gaussianprocess,rangeval;full_cov=true); #th
is function predicts the mean and covariance matrix depending on the data generat
ed from the Gaussian Process
boundary = meanval
combinedMeanGaussDmg=upwindDistr(rangevalue).*boundary #combining the
probability densities with the mean damage
Meanval = integrate(rangeval,combinedMeanGaussDmg) #calculating th
e mean of the Gaussian Process through the integration of the combined damage wit
h the wind speeds
Prob=[] #empty array to stor the probabilities
#for loop to generate the probabilities from the Weibull distribution
for i in 1:length(valrange)-1
    probability=quadgk(upwindDistr, valrange[i], valrange[i+1])[1]
    push!(Prob, probability)
end
Covariance=((Prob'.*Prob)*CovMtx) #calculating the covariance by multiply
ing the probabilities times the covariance matrix
StandDev=sqrt(sum(Covariance)) #calculating the standard deviation by
taking the square root of the sum of the covariance
GaussianPf=quadgk(z-
>cdf(LogNormal(miuD, sigmaD),z)*pdf(Normal(Meanval, StandDev),z), 0, Inf)[1]
# estimating the Gaussian failure probability by integrating the cdf function
of the log-normal with the pdf function of the gaussian normal distribution
GaussianReliability = 1-
GaussianPf #calculating the reliability of the Gaussian Process
return GaussianReliability, StandDev, GaussianPf
end
GaussianRel(R,v,d)

```

```
#Gaussian plot function

function GaussianPlot(z)
  y= linearInterpolation(v,d,z)
  kernel=SE(log(1.0),log(1.0))
  Mean=MeanZero()
  LogNoise = log(0.0)
  gaussianprocess= GP(z, y, Mean, kernel, LogNoise)
  gauplot = plot(gaussianprocess, xlabel="Wind Speed", ylabel="Mean Damage", title="Gaussian Process", label="Length Scale = 1.0", fillcolor = :green)
  return gauplot
end
GaussianPlot(R)
```